4-2019

The Acute Effects of Melatonin on Striatal Dopamine Release: Progressive Electrochemical Analysis in an Ex Vivo Mouse Model Utilizing Fast Scan Cyclic Voltammetry

Kevin D. Hughes
Grand Valley State University

The Acute Effects of Melatonin on Striatal Dopamine Release: Progressive Electrochemical Analysis in an *Ex Vivo* Mouse Model Utilizing Fast Scan Cyclic Voltammetry

Kevin D. Hughes

A Thesis Submitted to the Graduate Faculty of

GRAND VALLEY STATE UNIVERSITY

In

Partial Fulfillment of the Requirements

For the Degree of

Master of Health Science

Department of Biomedical Sciences

April 2019

Abstract

The caudate putamen is a sub region of the basal ganglia, containing neural tracts important for cognition, reward learning, and voluntary motor function. Dopamine (DA) signaling received from the dopaminergic neurons of the substantia nigra pars compacta mediate locomotion, degradation of which is the characteristic neuropathology for Parkinson's disease (PD). PD is an initially neurovegetative motor disorder but can progress to include cognitive impairments as well. Sundowner's syndrome (SS) has been observed in patient populations with neurodegenerative diseases, characterized by the decline of cognition into evening hours. Due to the circadian influence which the hormone melatonin has on the sleep-wake cycle, attention has been drawn to its relationship with SS. While melatonin has been observed to decrease DA release, the real-time measurement of acute melatonin exposure on DA release within the caudate has yet to be studied. Utilizing various techniques of fast scan cyclic voltammetry (FSCV) in an *ex vivo* mouse model, we observed a decrease in DA release upon exposure to supraphysiological concentrations of melatonin. Results from this experiment support previous literature suggesting that activation of presynaptically expressed melatonin receptor 1 (MT1) plays an important physiological role in downregulating DA release. Additionally, results suggest that 1-hour of MT1 activation is a sufficient time-frame for significant downregulation of DA availability. This research seeks to deepen understanding of the complex roles melatonin has on neurotransmission.

Table of Contents

List of Figures

List of Abbreviations

FSCV—Fast scan cyclic voltammetry

DA—Dopamine

CFme—Carbon fiber micro-electrode

V—Voltage

US—Unconditioned Stimulus

CS—Conditioned Stimulus

aCSF—Artificial cerebral spinal fluid

KCl—Potassium chloride

PD—Parkinson's disease

PDD—Parkinson's disease dementia

SS—Sundowner's syndrome

SCN—Suprachiasmatic nucleus

D1R—Dopamine 1-like receptor

D2R—Dopamine 2-like receptor

AC—Adenylyl cyclase

ATP—Adenosine triphosphate

cAMP—Cyclic adenosine monophosphate

PKA—Protein kinase A

VGCC—Voltage gated calcium channel

TH—Tyrosine hydroxylase

MT1—Melatonin receptor 1

Dmax—Peak current read from evoked DA release

GEE—Generalized estimating equations

IvT—Current versus time

Chapter 1

Early Zebrafish Trials

The Technique

Fast scan cyclic voltammetry (FSCV) has the ability to record the release of neurotransmitters from neurons in real time. FSCV works on the principle that some compounds, like dopamine (DA), are electroactive and capable of losing or gaining electrons given the right electrochemical conditions. By delivering a constant or cyclic voltage potential via a carbon fiber micro-electrode (CFme) inserted into nervous tissue we can create conditions to influence DA when to lose or gain its electrons while also simultaneously reading the movements they make. By measuring the magnitude of alternating current produced by these electron movements, we can quantify the concentration change of DA over time (Wassum & Phillips, 2015; Zachek, Hermans, Wightman, & McCarty, 2008).

DA belongs to a class of organic compounds called the catecholamines. containing a benzene ring with one side chain amine and two hydroxyl groups at the first and second carbon. As outlined in **Figure 1,** one electron is taken from each hydroxyl group when the oxidation potential is reached by the CFme, converting dopamine to dopamine-o-quinone and back into DA via oxidation-reduction reactions. Utilizing Demon Voltammetry Software (Wake Forest Innovations), the CFme is typically programmed to increase and decrease in voltage (V) in a linear and repeated fashion from the holding potential of -0.4V to the switching potential of +1.3V. DA experiences oxidation and reduction at voltage potentials of +0.6V and -0.2V, respectively compared

to a silver/silver chloride reference electrode. Utilizing software, the background current can be subtracted from what is read at the CFme, highlighting the difference in current across voltages and time allowing for the visualization of data as a background-subtracted color plot as shown in **Figure 2.** Historically, FSCV has proven itself to be a powerful electrochemical technique for measuring neurotransmitter release and reuptake in real time due to the sub-second temporal resolution of data collection.

DA is well documented as being a critical component in both physiological and cognitive processes (Marsden, 2006). FSCV is often used to deepen understanding of neurophysiological changes caused by environmental factors. Examples of this include observing the acute effects of certain psychoactive drugs on the release and uptake of neurotransmitters that play pivotal roles in the central nervous system (Ramsson, Howard, Covey, & Garris, 2011). However, FSCV can be used to observe the effects of learning as well. Demonstrated by previous studies, recording DA release can provide insight of what behavioral changes look like at the neurophysiological level.

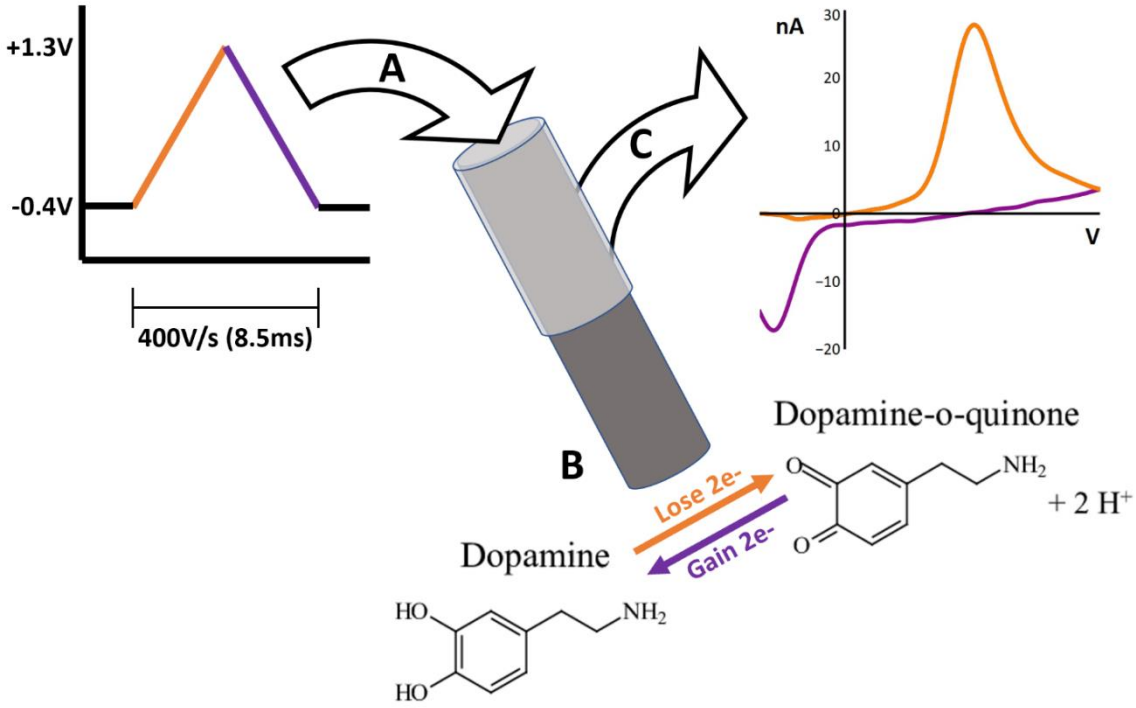

Figure 1. Basic FSCV principles: A cyclic voltage waveform is applied to the CFme (**A**), causing dopamine to lose and gain electrons (**B**). The current generated from these electron movements is then recorded and subtracted from the background current to produce a cyclic voltammogram (**C**).

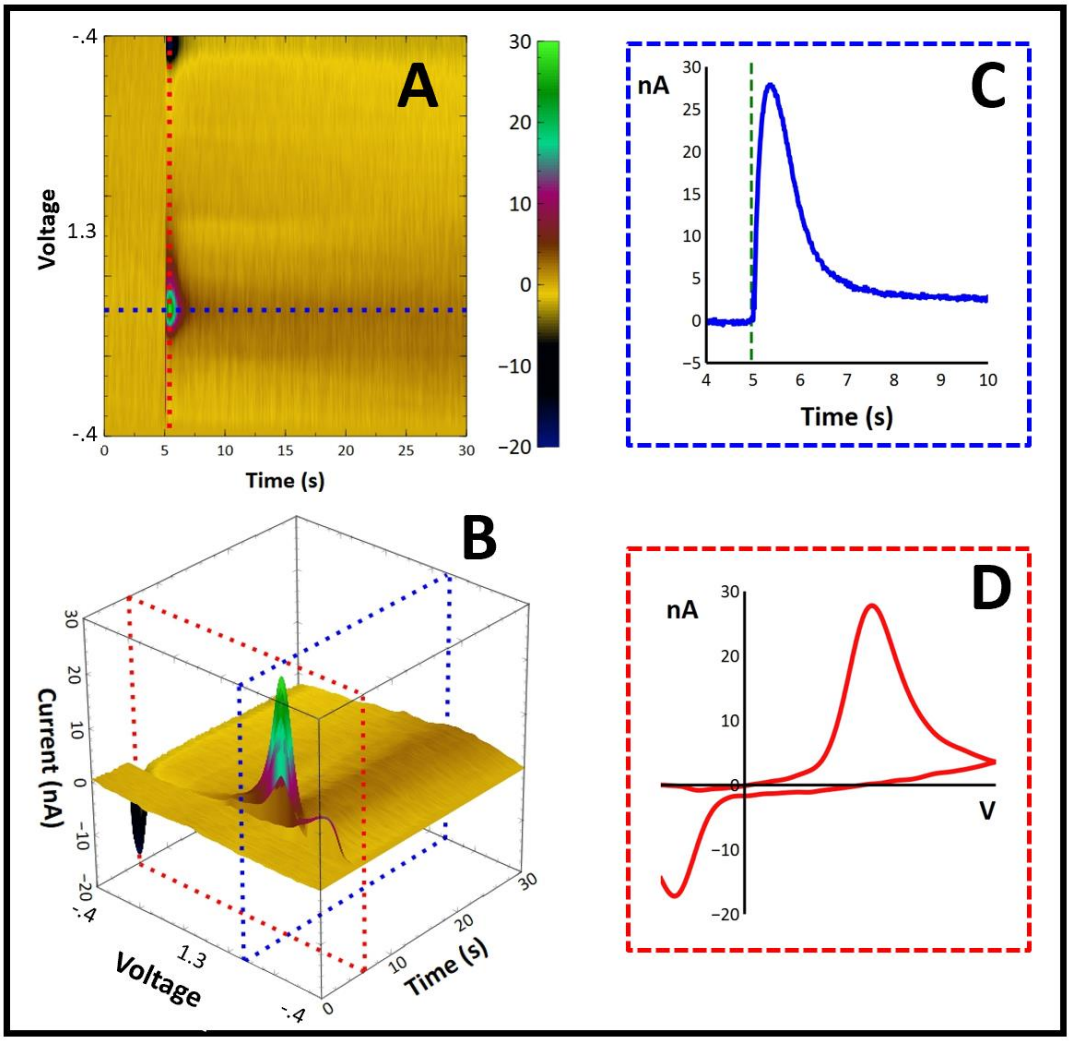

Figure 2. Background-subtracted color plot of stimulated DA release: A) 2D color plot of electrically evoked DA release. **B**) 3D representation of color plot in figure A. **C**) Current versus time graph at DA's oxidation potential, representative of the blue line which transects the color plots of figures A and B. **D**) Background-subtracted voltammogram just after tissue stimulation, representative of the red line which transects the color plots of figures A and B. Note DA's characteristic oxidation and reduction peaks. Time of stimulation occurs at 5 seconds, illustrated as the green dashed line in figure C.

Properties of Dopamine as a Neuromodulator

DA is one of several neurotransmitters that have secondary roles as neuromodulators, capable of effecting synaptic strength and membrane protein expression of individual neurons (Marder & Thirumalai, 2002). This modulatory property of DA and associated membrane proteins is essential to why it has been observed to have roles involved with the process of learning and memory. Synaptic strength can be upregulated or downregulated by many pre- and post-synaptic mechanisms resulting in physiological changes such as the amount of neurotransmitter released or rate of uptake (Owen & Brenner, 2012; Tellez, Gómez-Víquez, & Meneses, 2012). Measurement of DA release profiles utilizing FSCV allows for the indication that neuromodulation has occurred.

Flagel et al. (2011) explored reward learning in rats by observing phasic DA release in the mesolimbic system during operant conditioning. Upon receiving what the body deems as a desired stimulus such as food in this case (unconditioned stimulus, US), DA is released as a reward. Presenting rats with a push-lever (conditioned stimulus, CS) which provided the rat with food upon activation will lead to a shift in DA release from the US to the CS upon repetition. This reward learning process is fundamental for the reinforcement of actions and an organism's prediction of positive stimuli. FSCV was used to observe DA release in the nucleus accumbens core of rats during a Pavlovian training routine as described above. Repeated training sessions observed peak DA release to gradually shift from the US to the CS (Doya, 2002; Flagel et al., 2011; Ilango, Shumake,

Wetzel, Scheich, & Ohl, 2012). This experiment demonstrates the modulation of DA release in response to factors presented by the environment.

While studies such as Flagel et al. (2011) sought to observe changing DA profiles over a conditioning period, we hypothesized that we could compare the DA profiles of a conditioned animal versus an unconditioned animal. Through a training paradigm, we questioned if it was possible to promote learning to an extent that which the measurable DA release profile becomes significantly different than a control. With that research goal in mind we promptly began to seek out possible model organisms.

The Proposed Experiment

The methods for experimentation were inspired by a publication from a research group which was one of the first to explore the use of FSCV in *Danio rerio,* more commonly known as zebrafish (Jones, McCutcheon, Young, & Norton, 2015). Zebrafish are an appealing model organism since they possess a high degree of neurophysiological similarity to their mammalian counterparts. In addition to the physiological aspects, over 70% of human genes have an orthologue in zebrafish which together provide a foundation for effective human neurobehavioral disorder and disease modeling (Howe et al., 2013). Moreover, the lower costs of housing, feeding, and maintenance compared to popular mammalian model organisms was ideal.

Zebrafish are prominent model organisms used for studying learning and memory by displaying a capacity to learn avoidance and spatial paradigms under lab conditions (Naderi, Jamwal, Chivers, & Niyogi, 2016). Some conditioning studies may

administer a mild electric shock to the zebrafish as an US. Mitogen Activated Protein-mapping has indicated that the region of the brain which undergoes the most activity while being exposed to shock stimuli is the telencephalon (Randlett et al., 2015). Additionally, the dorsolateral and dorsomedial subsections of the telencephalon have been suggested to be the regions of the brain responsible for spatial learning and avoidance learning, respectively (Xu et al., 2012). Studies which have conducted anatomical imaging such as confocal microscopy and immunolabeling techniques have helped elucidate specific dopaminergic pathway locations within the zebrafish telencephalon which are suspected to be involved with avoidance learning and memory (Kaslin & Panula, 2001; Tay, Ronneberger, Ryu, Nitschke, & Driever, 2011).

We proposed that through experimentation we could measure evoked DA release in the dorsomedial telencephalon of control zebrafish utilizing FSCV. Then, after being subjected to an avoidance paradigm, test-group zebrafish would also have the same brain region analyzed. We hypothesized that the fish which were put through avoidance training would have a significantly greater DA profile than their control counterparts. However, simply the task to collect control data became an extended exercise in creativity and patience.

Data collection

We had hoped that the process of collecting voltammetry data would be straight forward. The framework for our methods of *ex vivo* data collection was initially very similar to Jones et al. (2015) as they appeared to be reasonably repeatable. Primarily

using Kaslin & Panula (2001) as an atlas for dopaminergic regions, many attempts were made to match location and depth of these regions. However, even placing the CFme in DA rich areas like the olfactory bulbs yielded no viable data.

Iontophoresis in tissue

Without any clear indication of DA release, the question arose if we were simply not administering a strong enough electrical pulse to elicit DA release or if our equipment was not sensitive enough to detect release events. Considering alternative methods brought us to the possibility of introducing DA into the system and then measuring the reuptake as a means to quantify change in synaptic strength. This is the fundamental basis of iontophoresis, i.e. discrete and controlled injection of drugs into tissue alongside a CFme for FSCV recording.

Electroactive compounds are dissolved in solution and injected into a capillary which has been pulled to create a type of pipette needle. A wire is inserted into the exposed and wider end allowing for the application of an electric current. The applied current by the wire will cause electrical migration of compounds out of the capillary and into the target environment (Herr, Daniel, Belle, Carelli, & Wightman, 2010). While preliminary buffer work showed some promising results, most attempts were inconsistent with DA having the tendency to leak out of the capillary uncontrollably. We concluded that the diameter of our manufactured pipettes was simply too wide for proper iontophoresis work. Without the means for more precise pipette manufacturing we sought alternative options.

Olfactory Stimulation

Upon referring to the literature we found a paper demonstrating use of olfactory stimulation to elicit DA release through the zebrafish's own neuronal circuitry. As mentioned previously, the olfactory bulb of the zebrafish is a region which is highly dopaminergic. Zebrafish receive olfactory input from a pair of nasal florets, akin to the olfactory epithelium in humans. By grinding fish food into a fine powder and mixing it into water we could create a solution which could be pipetted onto the fish's florets and cause an excitatory response within the olfactory bulb of the fish (Shang et al., 2015).

We adjusted our methods slightly so that we could accurately pipette food particles. The zebrafish was pinned in place within a 3D printed chamber which could be filled with artificial cerebral spinal fluid (aCSF) to nourish brain tissue through a reflected scalp. With the electrode inserted into the olfactory bulb we would begin recording and pipette food particles to the florets. Unfortunately, while the electrode did sometimes experience activity, we determined later that it was likely caused by pH changes in the environment, fish food reacting with the electrode, or the physical forces applied to the fish from food particle pipetting. Once again, we found ourselves without a viable option for collecting control data.

Inverted Microscopy

To eliminate possible cause of error, we began to reason that perhaps we simply did not possess the precision to accurately place the electrode. Through the university, our lab came to acquire an inverted microscope (Zeiss Microscopy) from another

department. With this inverted microscope we now had the ability to place a CFme with the spatial precision of single micrometers. In addition to our new equipment, we decided to explore evoking DA release through chemical stimulation as opposed to electrical. Flooding a tissue slice with aCSF containing a high concentration of potassium chloride (KCl) will create a strong ion imbalance across neuronal membranes which will in turn cause exocytotic release of neurotransmitters from axon terminals. This method has been used widely in the literature to elicit strong and continuous release of neurotransmitters (Heaulme, Leyris, Le Fur, & Soubrie, 1997).

Unfortunately, KCl proved difficult to work with and did not provide data of acceptable quality. Among other issues, introduction of a separate aCSF to our tissue flow chamber produced a pH change which affected our background signal and data recording. Additionally, we discovered the inverted microscope itself introduced electrical noise into our data recordings which made the interpretation of results difficult. Though we did produce a single data set which vaguely displays the redox profile of DA, the lack of repeatability questions its legitimacy as valid data. Eventually we decided that this too was unlikely to produce fruitful results.

Conclusions

Though much time was invested in searching for DA release throughout the zebrafish brain, all methods we tried were not viable. Whether it be issues with repeatability, manufacturing of materials, or simply lack of data, we concluded that we had truly exhausted our options. While it was difficult to accept defeat, the foundational

skills in voltammetry I had acquired allowed me to tackle the new techniques that were to come. I soon came to discover the excitement of scientific research in the project that followed and eventually became the main subject of this thesis.

Chapter 2

Introduction to Mouse Slice Work

Background

The catecholaminergic neurotransmitter DA has been well-documented to have important roles within the central nervous system. The basal ganglia of vertebrate species, including humans, is a group of subcortical nuclei within the forebrain containing neural tracts involved with voluntary motor function, cognition, and reward-learning pathways associated with habit formation. Classified as a subregion of the dorsal striatum within the basal ganglia, the caudate putamen receives signaling responsible for coordinating locomotion (Budygin et al., 2007; Hashemi et al., 2012). Studying DA insufficiencies within the striatum has become a particularly important topic among medical researchers due to its association with serious disorders such as Parkinson's disease (PD), primarily characterized by neuronal loss in the substantia nigra with dopaminergic denervation of the dorsolateral striatum (Dagher & Robbins, 2009; Mack et al., 2016). In the early stages of PD, the disease manifests itself as a motor disorder often causing bradykinesia, tremors, rigidity, and postural instability. However, later stages of PD sees patients experience cognitive dysfunction as well with up to 80% developing Parkinson's disease dementia (PDD), (Gratwicke, Jahanshahi, & Foltynie, 2015; Irwin et al., 2012; Mack et al., 2016). The physiological mechanisms of the non-motor symptoms of PD remain poorly understood (Mack et al., 2016).

A phenomenon which has been widely observed in the elderly with neurodegenerative disorders is the acute worsening of symptoms in the late evening and into the night. Increased confusion, hallucinations, agitation, aggression, anxiety, repetitive or disruptive vocalization, restlessness, and pacing or wandering have become characteristic of what is known as sundown syndrome (SS) (Cipriani, Lucetti, Carlesi, Danti, & Nuti, 2015; Hazelton, 2006; Silva, Sousa-Muñoz, Frade, Fernandes, & Magalhães, 2017). While neuropsychiatric symptoms for the syndrome have been well-documented, it lacks a clear definition and remains a descriptive term rather than a diagnosis (Canevelli et al., 2016; Silva et al., 2017). Although the precise neuropathology is still widely debated, much attention is drawn to the circadian nature which has been observed with SS.

Circadian rhythms are physiological cycles which occur in mammals roughly over a 24-hour period governed by the suprachiasmatic nucleus (SCN) of the brainstem. One of several biological processes under circadian control is the release of hormones in response to environmental lighting conditions to influence the sleep-wake cycle (Stone & Tranah, 2017). Via the retinohypothalamic tract, intrinsically photosensitive retinal ganglion cells within the retina convey light information directly to the SCN of the hypothalamus. From the SCN, projections carry circadian signaling to numerous brain regions, some of which mediate signaling further to endocrine tissues such as the pineal gland (Moore, 1995). While it has been discovered to be synthesized in small amounts among several tissues, the hormone melatonin is released most prominently by the pineal gland as part of the sleep-wake circadian rhythm. Its release is influenced by

environmental lighting conditions, with release generally being suppressed during the day and peak release being seen in the middle of the night (Kozaki, Kubokawa, Taketomi, & Hatae, 2015; Valdés-Tovar et al., 2018). The release of melatonin is most widely known to promote sleep, but studies in recent decades have begun to uncover the breadth of interaction melatonin has on various brain regions.

Melatonin Effects on Neurotransmission

The two major subclasses governing the receptor mediated communication between neurons upon DA release are the D1-like and D2-like (D1R and D2R) receptor families. The distinction is based on their downstream physiological effects upon activation. Both D1R and D2R belong to the family of seven transmembrane domain G-protein coupled receptors (GPCR) whose signal transduction pathways generally work in opposition of each other. D1R is exclusively expressed post-synapse, with ligand binding resulting in activation of adenylyl cyclase (AC). AC acts to convert adenosine tri-phosphate (ATP) into cyclic adenosine mono-phosphate (cAMP). High levels of cAMP allow for the activation of protein kinase A (PKA) which will go on to phosphorylate numerous proteins involved with metabolism, transcription, and ion channel function often directly relating to transduction of action potentials. The effects of D1R are viewed as excitatory in nature, as opposed to the effects of D2R activation (Vallone, Picetti, & Borrelli, 2000).

Though D2R has been observed to have heterogeneous post-synaptic expression in the striatum, we will be primarily discussing its more common role as a presynaptic

autoreceptor to focus on regulatory aspects of DA release. Acute activation of D2R primarily causes feedback inhibition of exocytotic release of DA from axon terminals. This response is mediated through G-protein βɣ-subunits which inhibit functionality of voltage-gated calcium channels (VGCC). Depreciation of calcium influx to the axon terminal inhibits the fusion of DA containing synaptic vesicles to the plasma membrane residing within the synaptic cleft. In other words, successive activation of D2R will reduce likelihood of continuous DA release from action potentials for a period lasting up to several seconds. Sustained activation of D2R will result in downregulation of AC, inhibiting intracellular cAMP levels and decreasing the abundance of PKA. The downstream effects of this include inactivation of tyrosine hydroxylase (TH), a rate limiting enzyme pivotal to the formation of DA precursor L-DOPA. Inhibition of DA synthesis will subsequently decrease DA availability for neurotransmission (De Mei, Ramos, Iitaka, & Borrelli, 2009; Ford, 2014; Vallone et al., 2000; Yapo et al., 2017).

Inhibitory effects of melatonin on mammalian dopaminergic release have been observed since the 1980's. Though the structure and function of melatonin receptors have been studied for decades, research uncovering melatonin's role in neurotransmission is more recent. Melatonin has been known to exert its physiological effects on the body through melatonin receptors 1 and 2 (MT1 and MT2). Like DA receptors, MT1 and MT2 belong to the extensive family of seven transmembrane GPCRs. Similar to D2R activation, the most well-defined signaling pathway for MT1 is the inhibition of intracellular cAMP accumulation via inactivation of AC (Dubocovich et al., 2010). These similarities suggest MT1 could produce similar downregulatory effects as

D2R depending on localized expression. Chronic activation of the MT1 receptor by circadian melatonin levels could possibly contribute to the known diurnal variation of DA availability (Ferris et al., 2014).

Past immunolabeling and cellular expression studies have established that the dopaminergic systems within the caudate putamen of both human and rodents express the melatonin receptor MT1. Moreover, MT1 and D2R are colocalized on the presynaptic Dopaminergic axon terminals which communicate within the caudate putamen (Uz et al., 2005). A recent study by Benleulmi-Chaachoua et al. (2015) sought to explain the mechanisms of action MT1 uses to attenuate VGCC activity which has been previously observed in the literature (Zisapel, 2001). It was confirmed that activation of striatal pre-synaptic MT1 receptors physically interact with VGCC of axon terminals to downregulate activity. As described above, inhibition of calcium influx will result in decreased DA release. Other striatal melatonin-mediated changes that have been reported include increased D2 receptor affinity (Hamdi, 1998). Function of the D1R, D2R, and MT1 receptors have been illustrated in **Figure 3**.

With this basis of knowledge, we should expect to see decreased stimulated DA release in the striatum of a mouse model upon melatonin exposure. However, real-time data on the time dependent effects which melatonin has on striatal DA release is yet to be observed. We propose the employment of FSCV as a tool to provide insight on the progressive decrease in DA release upon prolonged exposure to melatonin.

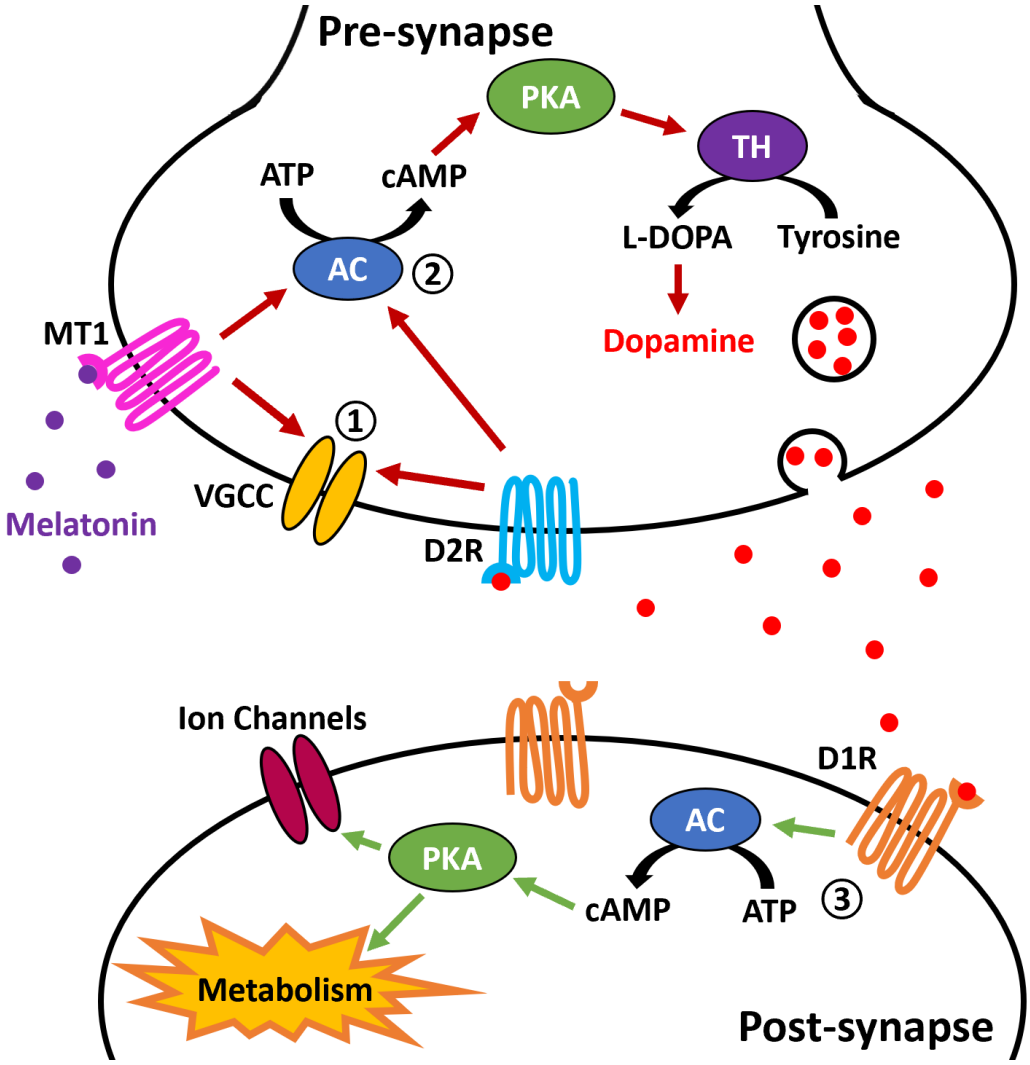

Figure 3. Receptor role in striatal DA release: The red arrows and green arrows represent a downregulatory and upregulatory response, respectively. (**1**) Acute activation of the D2R autoreceptor and MT1 receptor will result in inhibited function of the voltage gated calcium channel (VGCC). (**2**) Chronic activation of the D2R auto receptor and MT1 receptor will result in inhibited function of adenylyl cyclase (AC), decreasing cAMP accumulation and downregulating downstream enzymes important to DA synthesis. (**3**) D1R activation will upregulate AC, increasing cAMP accumulation allowing for an excitatory response altering cellular metabolism and ion channel function.

FSCV

As previously described in chapter 1, background-subtracted FSCV has shown to be an effective electrochemical technique for measuring neurotransmitter release and reuptake. Application of this technique is well-suited to the task at hand due to the high temporal resolution of real-time sub-second data collection (Hermans, Keithley, Kita, Sombers, & Wightman, 2008). Current is recorded in the order of nano-amps (nA); the amplitude of which correlates with the change in concentration of reactive analytes. Due to the diversity of oxidation potentials among organic compounds, the cyclic voltammogram for each electroactive neurochemical is unique. DA, for example, has become one of the most well-defined analytes in the field with known oxidation and reduction potentials being -0.2V and +0.6V, respectively.

FSCV can be utilized to detect DA concentrations upon electrically evoked axonal release within *ex vivo* tissue slices. Work with *ex vivo* tissue slices allow for simplified access to brain regions of interest and faster diffusion of drugs into tissue. However, there are some factors to consider when utilizing voltammetry. Complications in collection technique can arise when the drug of choice is also an electroactive compound.

Challenges of *ex vivo* FSCV

Melatonin is classified as an indolamine, a subclass of the monoamine neurotransmitters which include DA. Due to similar functional groups, melatonin is electroactive and capable of adsorbing to the CFme. It has been observed to cause

impedance, or fouling, of the CFme surface which results in decreased sensitivity to analytes (Hensley, Colley, & Ross, 2018). In order to reduce the confounding effects of fouling, three different voltammetry techniques will be employed. Consistency among the collection techniques will support the argument that what we observe is a biological effect and not misrepresented due to fouling.

The first method to be utilized will be a waveform used in fast-scan controlled-adsorption voltammetry (FSCAV). Developed by Atcherley et al. (2013), it is a technique originally designed to minimize DA adsorption to the CFme surface by increasing both the scan rate and frequency of the voltage waveform. We believe that by decreasing adsorption of DA we will also decrease adsorption of other analytes which would otherwise cause impedance of the CFme surface, like melatonin. One drawback to be expected from this waveform will be a decreased sensitivity to DA due to the decreased time available for adsorption between scans.

The second method will be the incorporation of a modified waveform designed specifically to eliminate fouling caused by melatonin developed by Hensley et al. (2018). This waveform increases both the holding potential and scan rate of typical values in order to minimize the effects of fouling of the CFme. While these modifications have proven to reduce the fouling effects of melatonin, a drawback which has been observed is the decreased sensitivity to DA. Even with this knowledge, the melatonin-specific waveform should still prove useful for observing any trends in DA release.

The final method to be explored will be the use of amperometry. Under specific conditions amperometry has certain advantages and limitations. As opposed to applying a cyclic voltage potential, amperometry operates by maintaining a constant voltage potential. Previous work has shown that melatonin reacts with the electrode at +0.8V. Therefore, by maintaining a constant voltage of +0.6V we can observe the oxidation of DA and eliminate the possibility of fouling. It should be noted that the lack of cyclic voltage potentials offers no selectivity of analytes. To ensure we will be observing DA, release sites in the tissue will first be found using a traditional waveform known to be more sensitive and selective to DA (Patel, 2008).

Tasimelteon

To provide additional support that the decrease in striatal DA release observed is a biological response to MT1 receptor activation, we utilized a melatonin receptor agonist. Tasimelteon has been used clinically since 2014 as an orally administered MT1 and MT2 receptor agonist to treat sleep disorders. Though tasimelteon has a slightly reduced binding affinity to MT1 compared to melatonin, preliminary voltammetry work highlighted its experimental viability through relatively minor interaction with the electrode surface. Tasimelteon will be used to demonstrate that observed striatal DA release is not merely a product of electrode fouling and rather a function of MT1 activation (Dhillon & Clarke, 2014).

Relevance and Purpose

The primary purpose of this study is to elucidate the acute neurobiological effects of melatonin exposure on the release of DA within the caudate putamen of a mouse model. While previous studies have utilized protein assays to study melatonin exposure on cellular activity, we propose an *ex vivo* approach. By inserting the CFme directly into the caudate putamen of mouse brain slices for FSCV recording we will be able to progressively record DA release over a defined period of melatonin exposure. In order to elicit the strongest response, we hope to saturate MT1 and MT2 receptors by using multiple supraphysiological concentrations of melatonin in a range inspired by the work done by Paredes et al. (1999).

The evidence presented by the literature suggest that melatonin decreases striatal DA release from dopaminergic axon terminals which express the MT1 receptor. For a clinical application this could present an argument that the administration of melatonin to an individual with PD would be ineffective for treatment due to the already existing DA insufficiency which is rooted in the neuropathology of the disease. While we are not explicitly researching PD, the research conducted in this experiment could still add knowledge to the field of research exploring the therapeutic potential of melatonin on neurodegenerative diseases or neuropsychiatric disorders.

Clinical studies on the application of melatonin for the treatment of neurodegenerative disorders has had mixed results. As described in Trotti & Karroum (2016), recent studies have shown that using melatonin to treat patients with

neurodegenerative diseases such as Parkinson's fail to produce therapeutic results for treating motor PD (Pandi-Perumal et al., 2013; Willis & Armstrong, 1999) but show some antidepressant effects and sleep disorder improvement (Bassani et al., 2014). However, melatonin has shown to attenuate Dopaminergic neuronal cell death in a rotenone induced PD rat model (Carriere, Kang, & Niles, 2016) and a 6-hydroxyDA induced PD rat model (Yildirim et al., 2014). Promising results have also been observed in induced PD mouse models when supplemental melatonin was administered with L-DOPA (Naskar et al., 2013; Zaitone, Hammad, & Farag, 2013), likely attributed to melatonin's natural role as an antioxidant for the reduction of oxidative stress seen by mitochondria in PD (Patki & Lau, 2011).

Chapter 3

Materials and Methods

Carbon Fiber Micro-Electrodes

Carbon fiber micro-electrodes were fabricated using 7μm T-650 carbon fiber (Cytec Engineering) thread into a glass capillary tube (0.68mm ID/ 1.2mm OD) and pulled in a capillary puller (Sutter P77). Exposed carbon fiber was cut to a length of 50-100μM and sealed in epoxy resin or paraffin wax then briefly washed with acetone or xylene, respectively.

Animals

Adult male C57BL/6J mice (Jackson Laboratories) were housed under a 12-hour day/night cycle with food and water available *ad libitum*. Mice selected for experimentation were anesthetized using isoflurane (1.5%, 2L/min O_2) and then euthanized via cervical dislocation. The intact brain was removed from the skull via dissection and placed in ice-cold artificial cerebral spinal fluid (aCSF) buffer bubbled with carbogen (95%O_2/5%CO_2) and containing the following (in mM): 126 NaCl, 2.5 KCl, 1.2 NaH_2PO_4, 2.4 $CaCl_2$, 1.2 $MgCl_2$, 25 $NaHCO_3$, 11 glucose, and 0.4 l-ascorbic acid. A vibratome (Campden Instruments) filled with the same aCSF buffer was used to obtain 300μm thick sagittal cross-sections of the brain. Slices were allowed to rest at room temperature while supplied with a constant flow of aCSF buffer until ready to use. All procedures were approved by and in compliance with the Grand Valley State University Institutional Animal Care and Use Committee.

Ex Vivo FSCV in Brain Slices

Slices of mouse brain containing portions of the caudate putamen were placed in a 3D-printed flow chamber and held in place with a slice harp (Warner Instruments). aCSF buffer was continuously bubbled with carbogen and heated to 37°C before flowing through the chamber at a rate of approximately 1mL/min. Slices were given 1 hour to acclimate before FSCV work began, allowing for simultaneous preparation of the electrodes. Before tissue entry, electrodes were first submerged in the flowing aCSF and cycled for 15 minutes at 60Hz to clean the electrode surface, a protocol inspired by Takmakov et al. (2010). CFme were then lowered into the target tissue just until the entirety of the CFme was below the surface. DA release was electrically evoked via stimulation electrodes placed on the surface of the tissue slice on either side of the CFme entry site (**figure 4**). Recordings lasted 30 seconds with a stimulus onset delay of 5 seconds, an intensity of 350uA, 1 pulse, 60Hz monophasic stimulation. Each trial consisted of 5 pre-drug recordings, 12 recordings during drug exposure, and 12 recordings of post-drug washout. Melatonin concentrations of 10μM, 50μM, and 100μM were added to aCSF buffer and were exposed to the tissue during drug exposure periods. All recordings were given 5-minute refractory intervals to allow for the tissue to equilibrate. Experiments were also dedicated to observing the effects of 100μM tasimelteon exposure.

An n=3 was collected for each melatonin concentration for each waveform. Pseudo-replication was avoided by ensuring that brain slices from a mouse were not exposed to the same concentration of melatonin twice. Parameters for FSCAV collection

maintain the same holding (-0.4V) and switching (+1.3V) potentials as traditional FSCV recording but increase the scan rate to 1200V/s with a frequency of 100Hz. For the melatonin specific waveform, a holding potential of +0.2V and a switching potential of +1.3V was utilized with a scan rate of 600V/s and frequency of 10Hz. Finally, amperometry was employed to hold a constant voltage potential of +0.6V at 60Hz to reduce melatonin fouling. When preparing to collect data with the melatonin-specific waveform and amperometry, DA release sites were first sought out using the traditional FSCV waveform (-0.4V-1.3V, 400V/s, 10Hz) due to high sensitivity to DA.

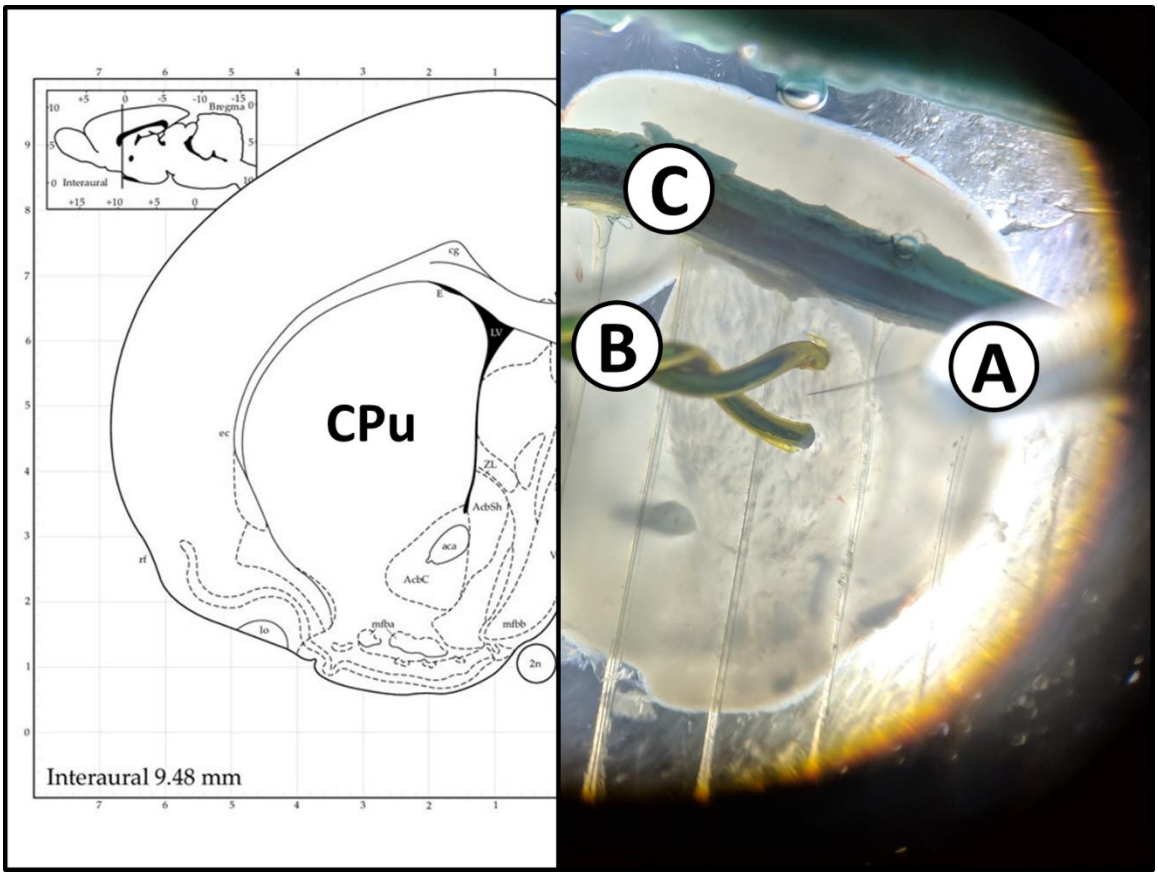

Figure 4. Experimental Setup – Electrode Placement: The left side of this figure is from a mouse brain atlas by Franklin & Paxinos (2008) used for reference when collecting brain slices. The right side of this figure is an image taken during experimentation, note the central location of the caudate putamen (CPu) on both sides of this figure. The CFme, located at the end of a pulled capillary (**A**) was positioned between two stimulating electrodes (**B**). The brain slice was immobilized with the aid of a metal slice harp with lycra strings (**C**).

Voltammetry in vitro

Electrodes were saved after *ex vivo* work to be calibrated with 1uM DA to quantify electrode sensitivity. The electrodes were placed in a thin flow chamber submerged in calibration aCSF containing the following (in mM): 126 NaCl, 2.5KCl, 0.66 NaH_2PO_4, 2 Na_2HPO_4, 2.4 $CaCl_2$, 1.2 $MgCl_2$, 11 glucose, and 0.4 l-ascorbic acid. The calibration aCSF pH was manually adjusted to 7.4 before it was used for electrode calibrations. Calibration recordings spanned a duration of 30 seconds, with calibration aCSF containing an additional 1μM DA timed to enter the flow chamber at approximately 10 seconds and be exposed to the electrode for roughly 10 seconds. Electrodes utilized the same waveforms used during experimental data collection. Calibrations were run until multiple consistent peak amplitudes for DA were produced.

Additional FSCV work

Demonstration of melatonin interaction with the CFme utilizing the traditional FSCV waveform was carried out. An experimental environment was simulated by continuously exposing the CFme to an aCSF buffer containing 10μM melatonin with the addition and subsequent removal of 1μM DA in 5-minute intervals. A pipette-based calibration technique was utilized for DA introduction to the CFme, inspired by Ramsson (2016).

Statistical analysis

The peak current produced by DA release (Dmax) was noted for each recording. To normalize data for statistical analysis, the 5 pre-drug recordings were averaged and

the remaining values for the drug exposure and washout periods were expressed as a ratio (%) of the pre-drug average. The relative ratios for each experimental group were then combined allowing for simplified analysis of statistical significance between data sets. Upon consultation with a statistician we decided on the utilization of generalized estimating equations (GEE) for the statistical analysis which was performed in SAS (version 9.4). For each of the two experimental recording periods, drug exposure and washout, the significance of change in Dmax was compared as a function of waveform, concentration, time, and combinations of these variables.

Graphing

Raw data for background subtracted voltammograms, current verses time (IvT), and background current were output from files recorded in Demon Voltammetry Software (Wake Forest Innovations). All data was imported to and graphed utilizing Veusz graphing software.

Chapter 4

Results & Discussion

Summary of Results

Figure 5 displays the average relative ratio of Dmax for each concentration of melatonin and respective waveforms used. Time -20 to 0 minutes represent the 5 pre-exposure recordings before the introduction of melatonin to the brain slice. At time 0, brain slices were exposed to a 10μM, 50μM, or 100μM concentration of melatonin for 60 minutes where 12 recordings were taken at 5-minute intervals. The final 12 time points, 65-120 minutes, span the drug washout period when melatonin has been removed from the incoming aCSF buffer. Dmax endpoints for the melatonin exposure and washout period have been compiled in **Table 1** (**Appendix A**).

Upon initial assessment of the graphs, it is apparent that in most cases Dmax experiences a decrease upon melatonin exposure with varying responses to the washout period. We expected a dose-dependent response overall, but the data shows the melatonin-specific waveform and amperometry experienced a slightly greater mean decrease in Dmax with 50μM melatonin than 100μM. Additionally, change in Dmax across all waveforms appeared to have similar profiles under the influence of 50μM and 100μM melatonin. The statistics support this initial observation.

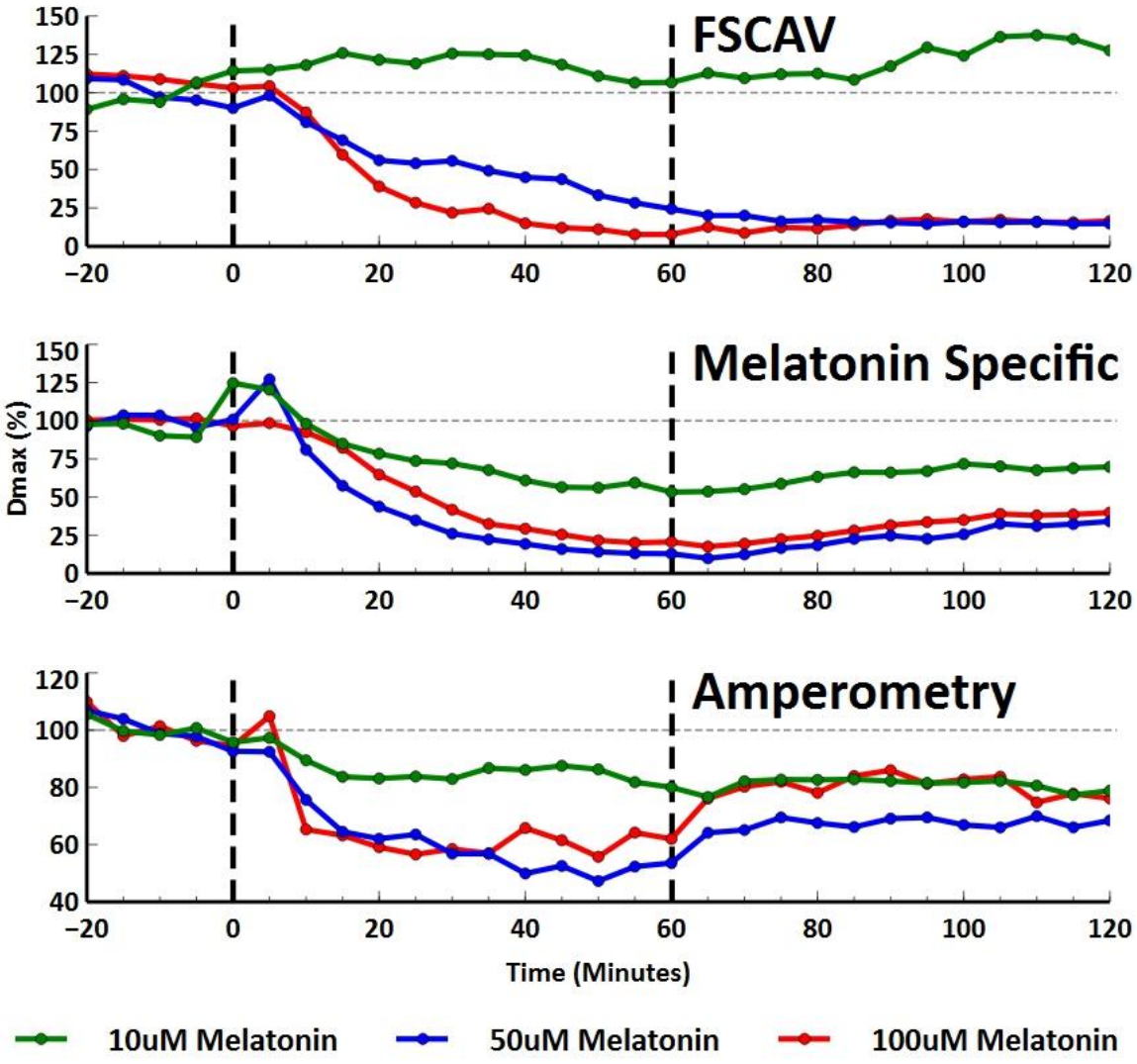

Figure 5. Results Summary by Waveform: The mean Dmax for each melatonin concentration group has been plotted as a ratio of the 5 pre-exposure recordings (-20-0 minutes). The melatonin exposure period occupies the time from 0 to 60 minutes, and the washout period occurs from 60 to 120 minutes. The beginning and end of melatonin exposure to the brain slice is marked with a dashed black line.

Statistical Results

Tables 2 and 3 (**Appendix A**) outline the factors for which significant change in DA release is dependent upon using 100μM melatonin as a baseline. Upon observing DA release during melatonin exposure as a function of time and concentration across waveforms, GEE parameter estimates returned a p-value of 0.6835 for 50μM and a p-value of 0.0081 for 10μM (**Table 2**). These results show that across waveforms, the trend of Dmax upon exposure to 100μM melatonin does not significantly differ from 50μM but does significantly differ from 10μM. However, as displayed in **Appendix A, Table 3** this trend does not continue into the washout period as 100μM does not differ from either 50μM (P=0.5371) nor 10μM (P=0.9765).

Wald statistics for GEE analysis are outlined in **Tables 4 and 5** (**Appendix A**). Significance of DA release as a function of time, concentration, and waveform had the greatest effect during the exposure period, seen by a P-value of 0.0043 (**Appendix A, Table 4**). This same effect, however, was not shared by the washout period as analysis yielded a P-value of 0.1304 (**Appendix A, Table 5**). These results indicate that overall observed change in Dmax over the course of the melatonin exposure period is heavily dependent on time, but during the washout period time does not hold the same effect. If the decrease in DA release observed was primarily attributed to fouling, then we would expect the signal to recover during the washout period as melatonin leaves the environment. This evidence supports the notion that the change in DA release observed is the result of a biological effect of melatonin on the dopaminergic axon terminals as opposed to fouling of the electrode.

Figures 6 and 7 represent the predicted linear model derived from GEE parameter estimates summarized in **Tables 6 and 7**, respectively (**Appendix A**). Observing the data as predicted linear models allows for a clearer and, more importantly, statistical lens through which we can observe results. Graphed in **Figure 6**, it is apparent that every concentration of each waveform during the melatonin exposure period exhibits some degree of negative slope over time indicating an overall decrease in Dmax. Considering the strong interaction that time has during this period as indicated by the Wald statistics, this representation is consistent with what we would expect while also displaying which group experienced the greatest decline in predicted Dmax.

Observing the interaction of waveform and concentration on Dmax at each time point offers insight to how soon melatonin causes significant differences between test groups during the exposure period. Outlined in **Table 8 (appendix A)** are the Wald statistics for each time point. We can see that the P-values dip below 0.05 as soon as 25 minutes into the exposure period and remain so for the duration of the hour with the one exception at 35 minutes. Based on this experiment, the data indicates that statistically significant change in Dmax upon melatonin introduction does not occur until at least 25 minutes into exposure. As previously described by the Wald statistics in **Tables 4 and 5**, the strong interaction of time does not carry into the washout period.

Figure 7 graphically represents the washout period which displays more gentle slopes than the exposure period while also exhibiting the lack of unidirectional slopes. This is the resulting behavior when significant change does not occur over the time course, reiterating the lack of strong interaction of time on change in Dmax. As

mentioned previously, lacking the significant interaction of time opposes the likelihood that fouling of the electrode surface is the primary contributor to the observed decrease in Dmax in the exposure period. All the waveforms utilized were chosen for their properties which reduce the fouling capacity of melatonin. With its constant holding potential, amperometry was expected to be the least susceptible to fouling by melatonin. Upon closer inspection of **Figure 7**, the three linear functions with the smallest slope all belong to the melatonin concentrations tested using amperometry. Disregarding time and observing Dmax as a function of concentration and waveform, statistical analysis finds that these linear functions are extremely similar to each other (**Table 9, Appendix A**). Considering the near-absent effect that melatonin washout has on amperometry, it becomes increasing likely that the decrease in Dmax observed using amperometry during the melatonin exposure period is indeed a result of biological function. As for the other waveforms, insight on the presence of fouling can be gained from analyzing the voltammetry data.

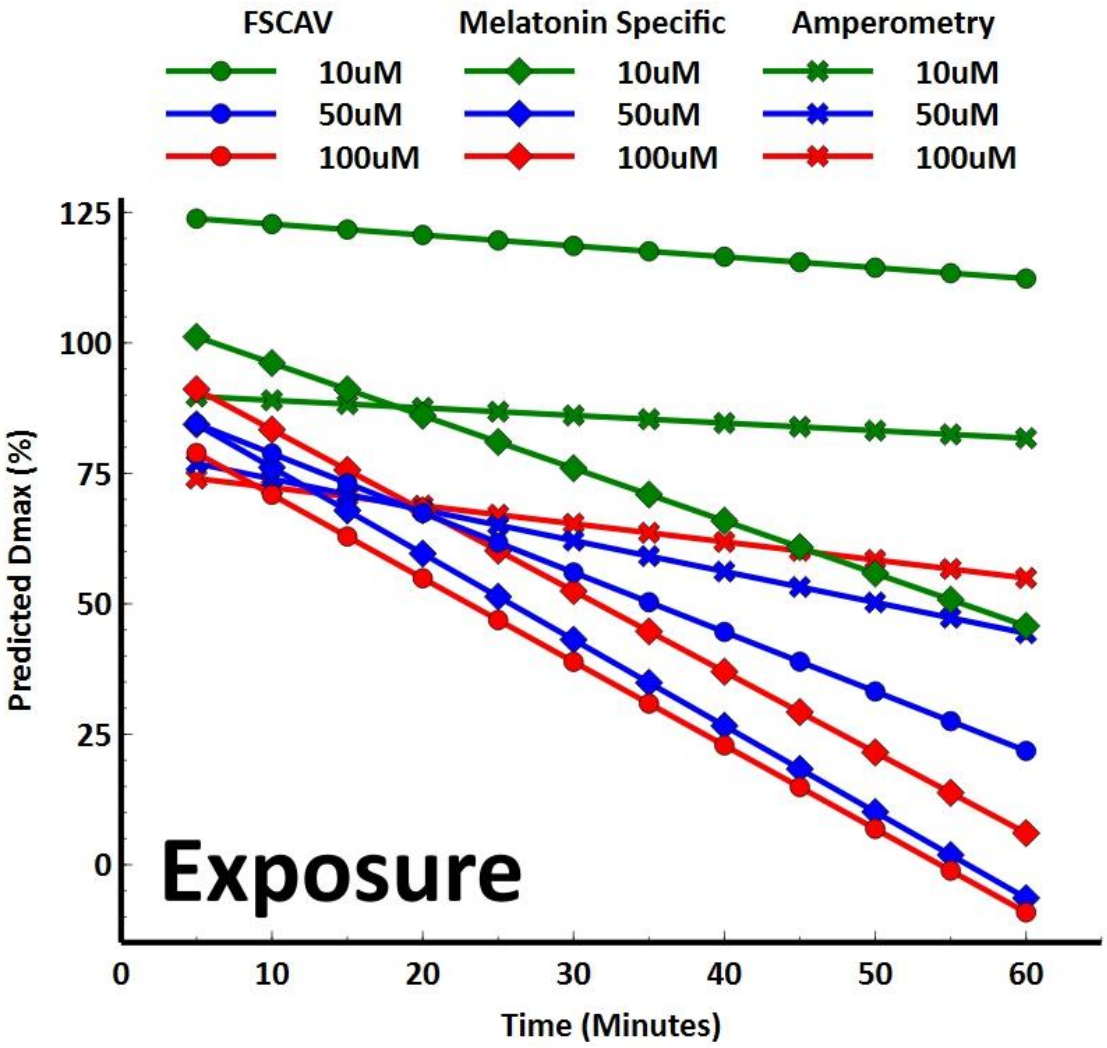

Figure 6. Predicted linear model of melatonin exposure period derived from GEE parameter estimates

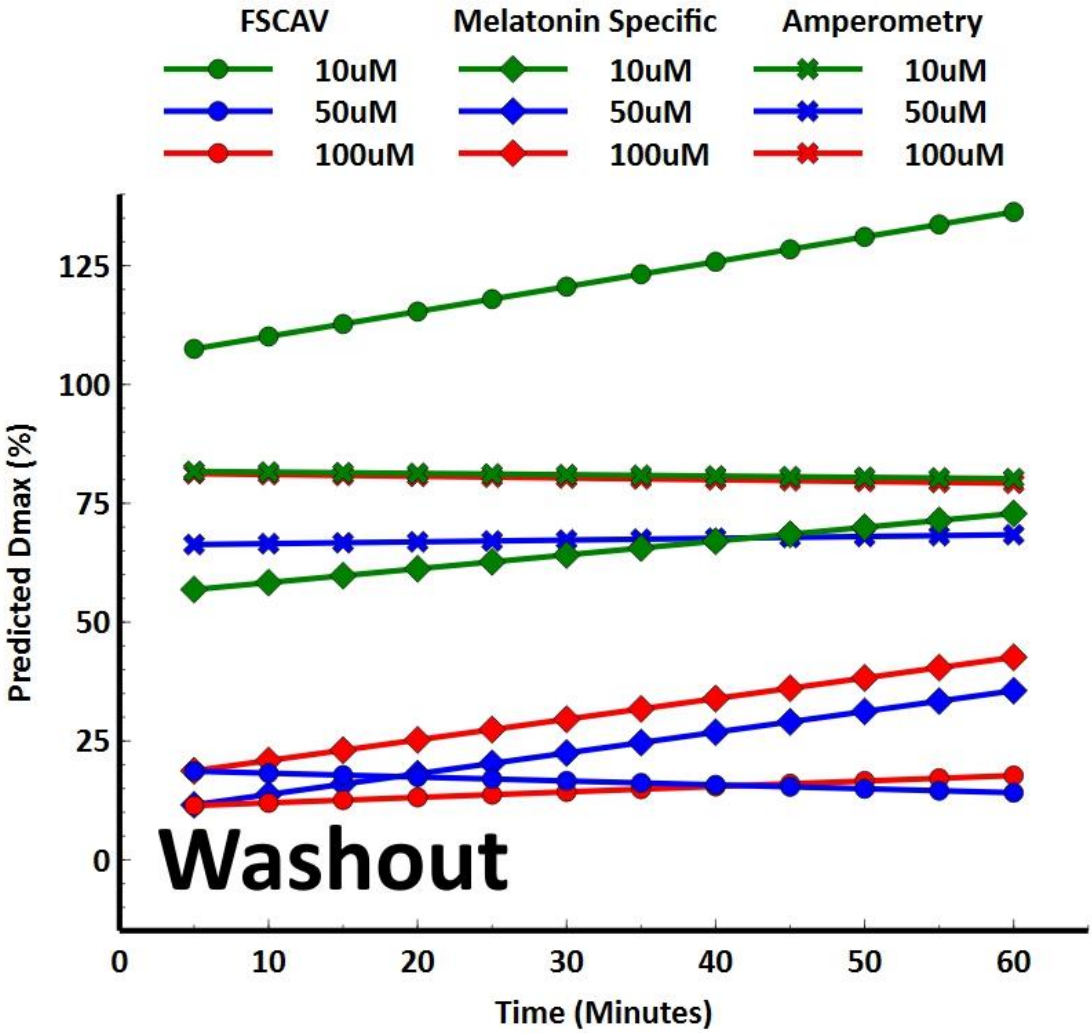

Figure 7. Predicted linear model of melatonin washout period derived from GEE parameter estimates

Voltammetry Data

Figures 8 and 9 display the voltammetry data recorded utilizing the FSCAV waveform for 10μM, 50μM, and 100μM melatonin concentrations respectively. While the changes in current amplitude of the cyclic voltammograms and IvT plots between experimental periods is the most immediately apparent feature, the data has already been summarized in **Figure 5**. What we are interested in are the properties that indicate impedance as explored by Meunier, Roberts, McCarty, & Sombers (2017). Their research shows that impedance will cause a decrease in sensitivity as well as a positive shift in voltage potential required for redox reactions of DA. **Figure 11** illustrates voltammetry data from experiments utilizing the FSCAV waveform and melatonin specific waveform which exposed brain slices to the 100μM melatonin concentration. If either of these waveforms are susceptible to melatonin fouling, the evidence will present itself at our highest concentration. Positive shifts in the oxidation potential can be observed for both the FSCAV (**Figure 11A**) and melatonin specific (**Figure 11B**) waveforms with the background and background-subtracted plots experiencing a minor positive shift as well. While this evidence may initially seem contradictory, comparison to voltammetry data of CFme exposure to only 10μM melatonin utilizing the traditional FSCV waveform provides perspective on the oxidation shift which severe fouling can cause (**Figure 12A**). Although it is true that these two specialized waveforms still experienced a small degree of fouling, the relatively minor change in oxidation potential reveals that fouling likely had only a small effect on the decrease in Dmax observed. Though we are unable to quantify how much of the change in Dmax observed can be attributed to fouling due to

our methods of collection, minor observed impedance coupled with a lack of a time-dependent change during the washout period indicates fouling present was minimal.

The progression of change in aspects of voltammetry recordings over the course of the experiments have been outlined in **Figures 8, 9, and 10**. The background plot, cyclic voltammogram, and IvT plot for each concentration of melatonin has been selected from an experiment which best represents the mean Dmax of that respective group. The three data sets plotted on each graph represent the final recording of the pre-melatonin, melatonin exposure, and melatonin washout periods. Observing how these recordings change from exposure to washout periods provide insight to activity occurring at the electrode surface.

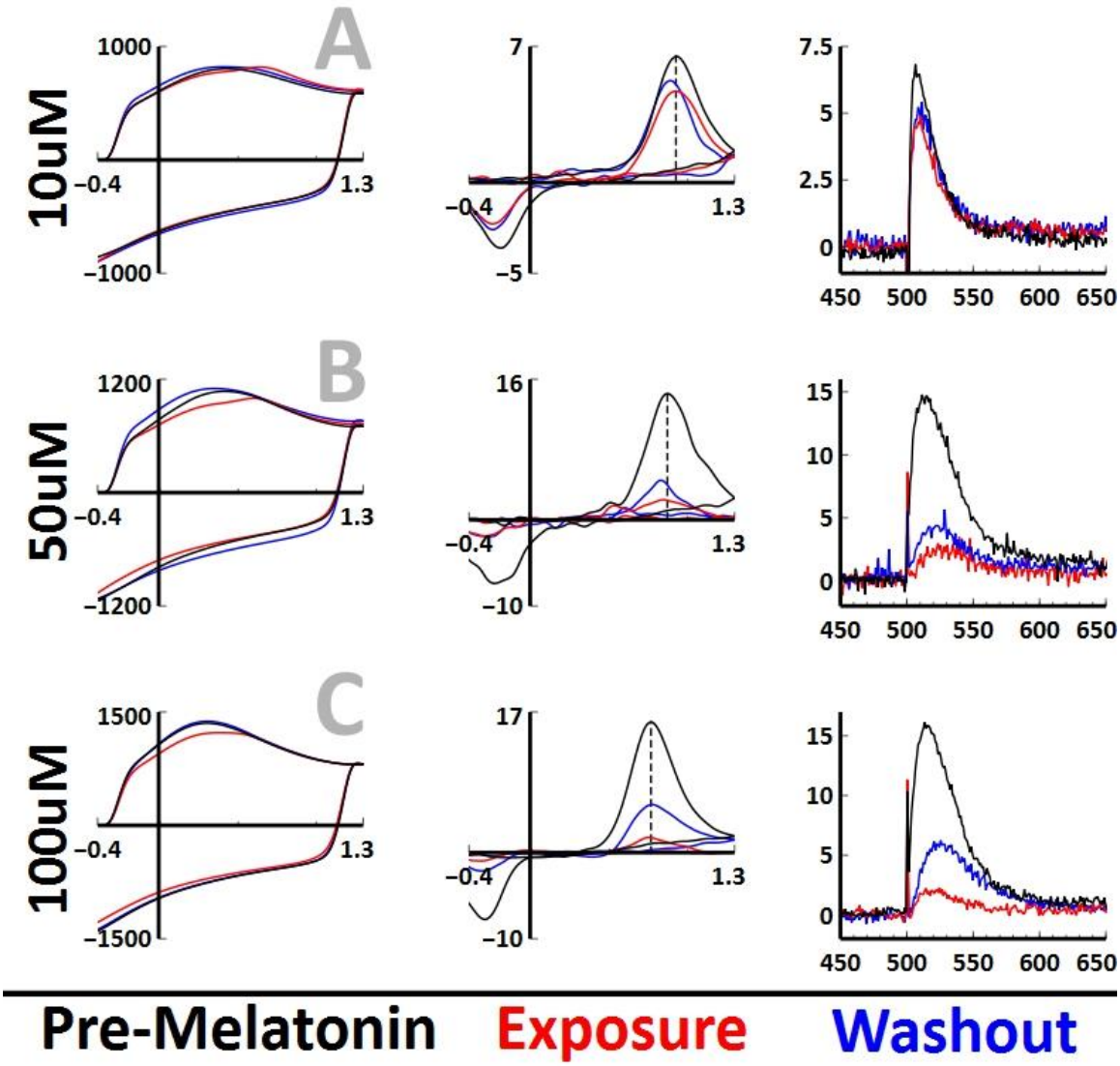

Figure 8. Data Collection Utilizing FSCAV Waveform: Background, background-subtracted voltammogram, and current over time for 10μM (**A**), 50μM (**B**), and 100μM (**C**) melatonin exposure, respectively. For each graph the black line, red line, and blue line represent the final recording for the pre-melatonin, exposure, and washout experimental periods respectively.

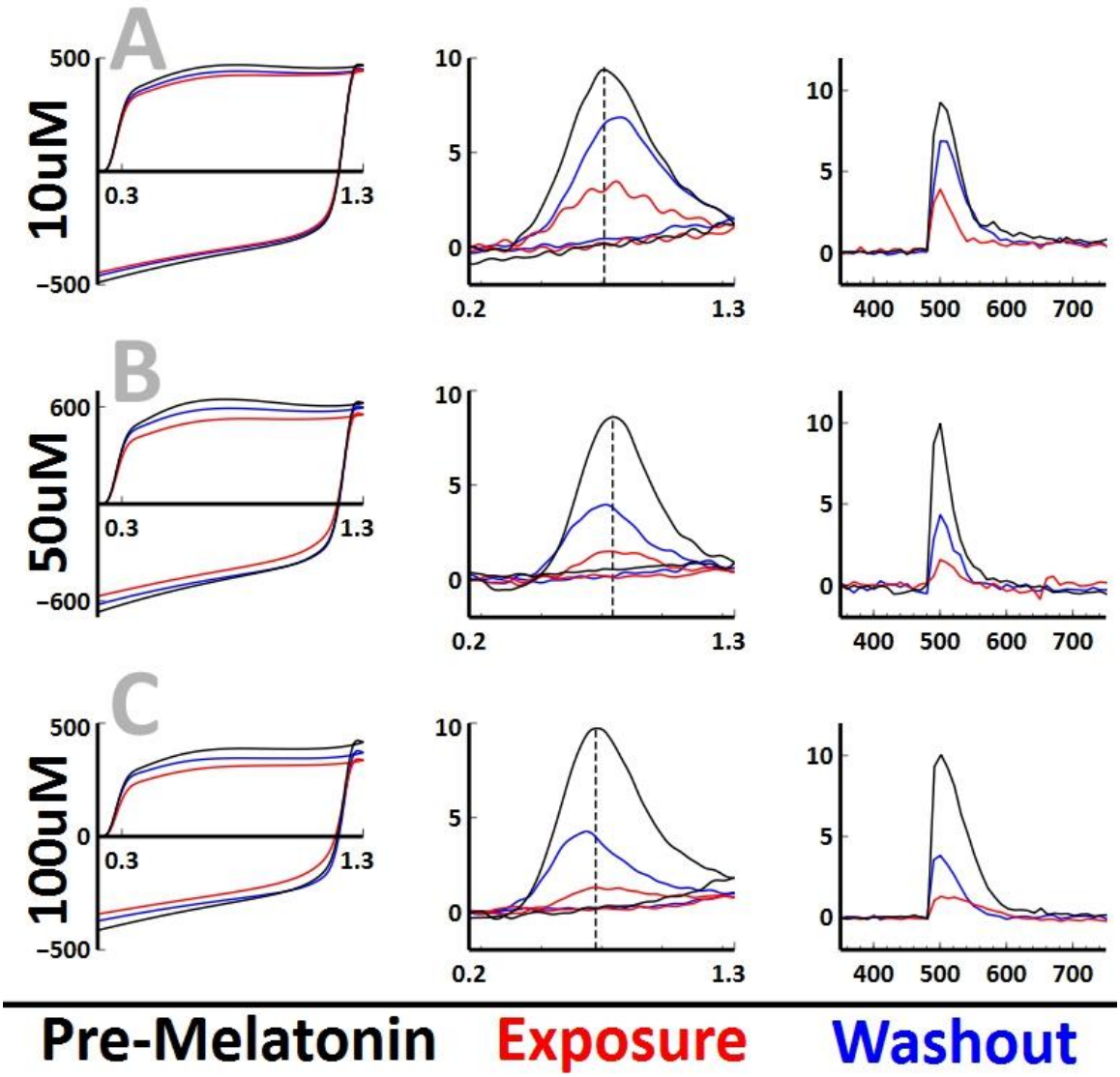

Figure 9. Data Collection Utilizing Melatonin-specific Waveform: Background, background-subtracted voltammogram, and current over time for 10μM (**A**), 50μM (**B**), and 100μM (**C**) melatonin exposure, respectively. For each graph the black line, red line, and blue line represent the final recording for the pre-melatonin, exposure, and washout experimental periods respectively.

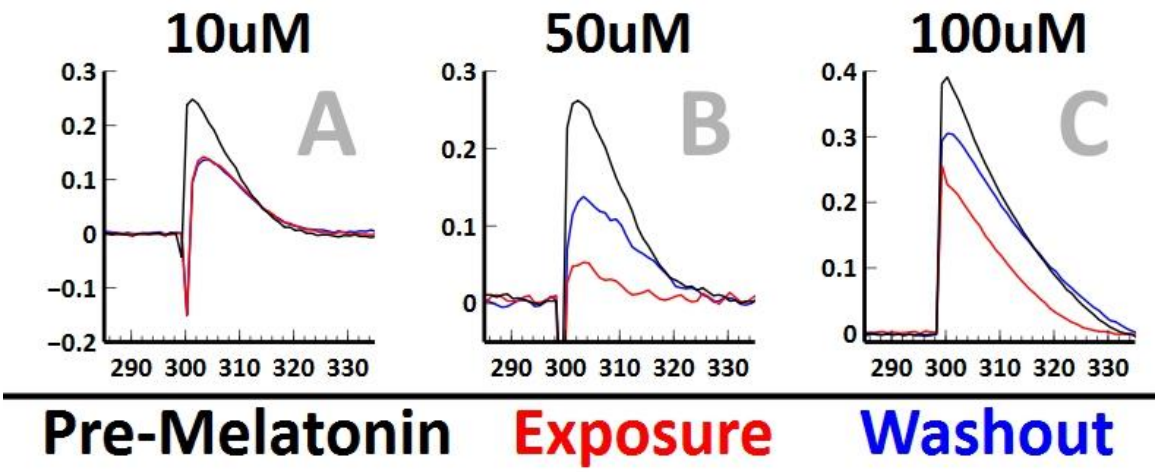

Figure 10. **Data Collection Utilizing Amperometry:** Current over time graphs for 10μM (**A**), 50μM (**B**), and 100μM (**C**) melatonin exposure. For each graph the black line, red line, and blue line represent the final recording for the pre-melatonin, exposure, and washout experimental periods respectively.

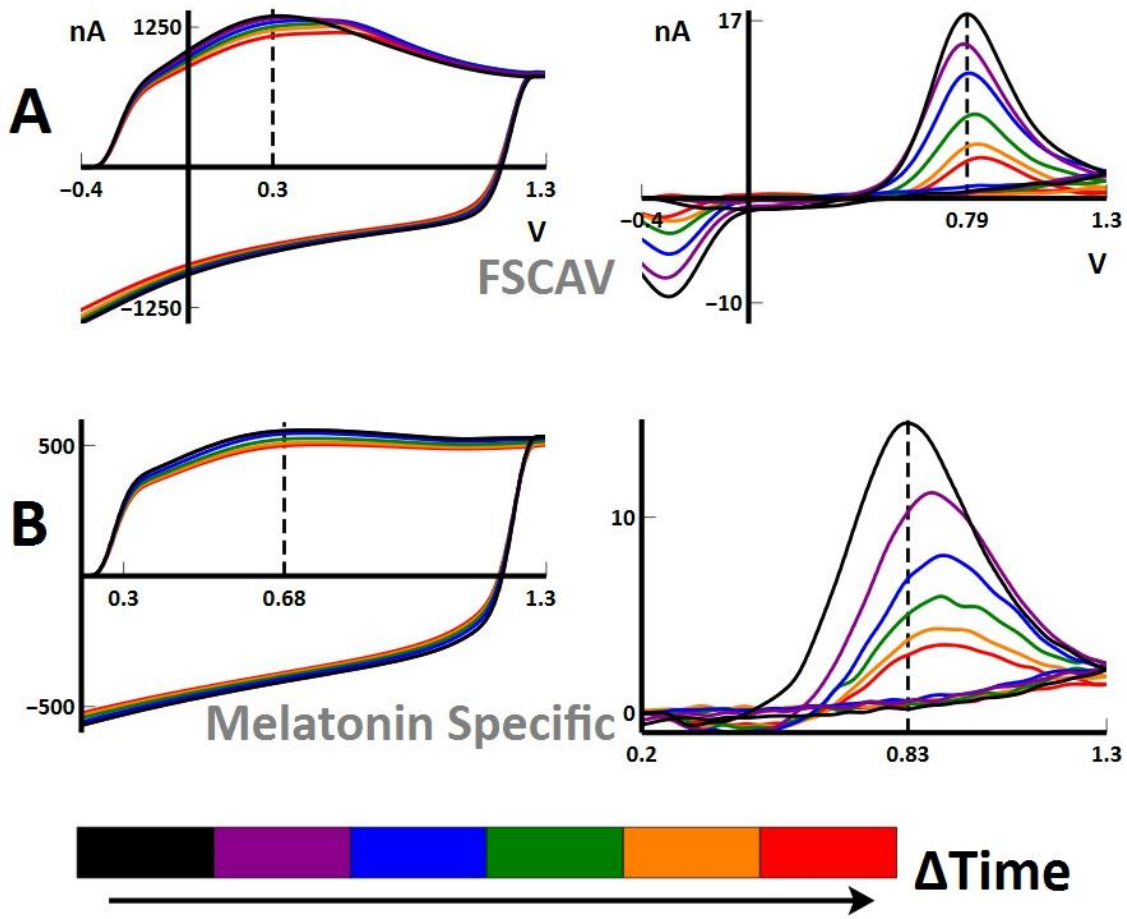

Figure 11. Progression of DA oxidation behavior during melatonin exposure utilizing tested waveforms: Background (left) and background-subtracted (right) cyclic voltammograms have been plotted to observe any susceptibility that the FSCAV (**A**) and melatonin specific (**B**) waveforms may have to melatonin fouling at 100μM. The dashed line represents the DA oxidation potential of the first recording (black). Subsequent recordings are colored to reflect the progression of time until concluding with red.

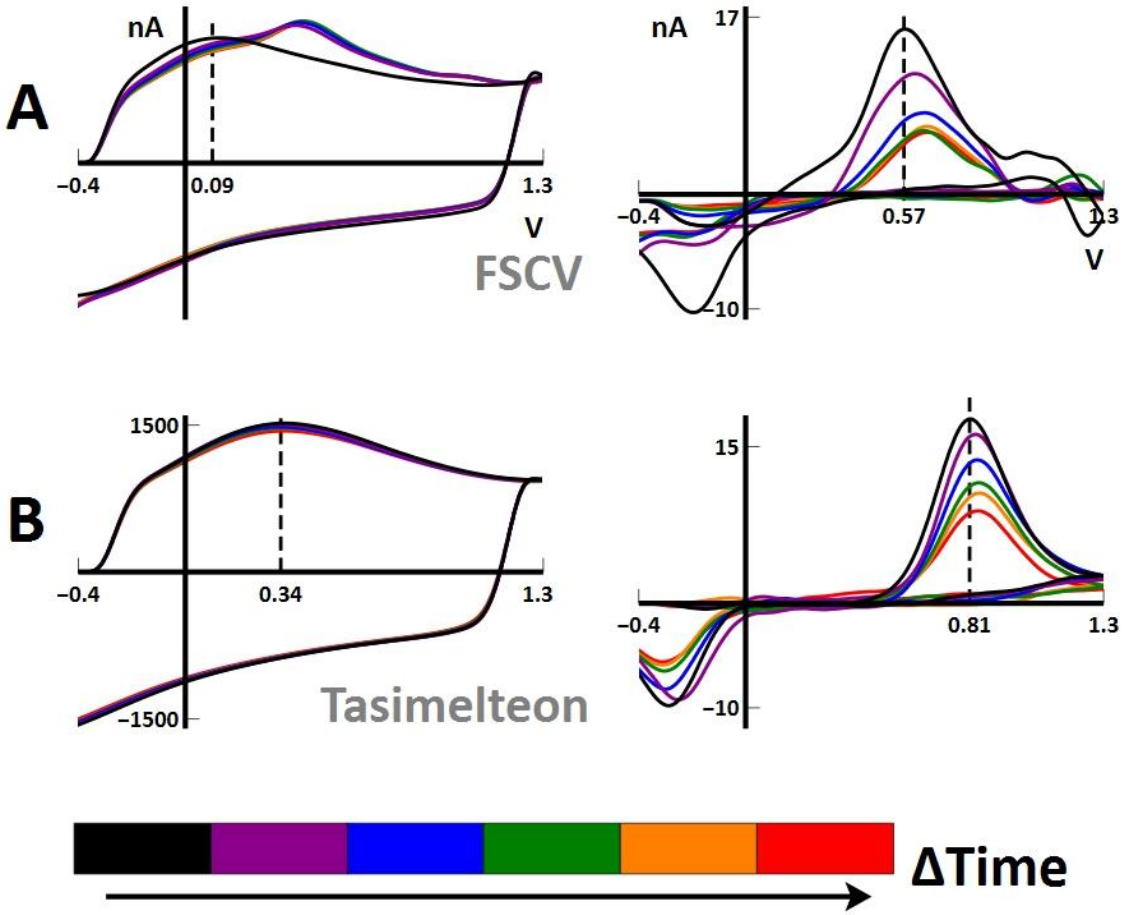

Figure 12. Comparative progression of DA oxidation behavior during melatonin exposure: Background (left) and background-subtracted (right) cyclic voltammograms have been plotted to observe susceptibility that the traditional FSCV waveform (**A**) has to melatonin fouling at 10μM in aCSF buffer. MT1 agonist tasimelteon (**B**) exposure to mouse brain tissue slice, read with FSCAV waveform. The dashed line represents the DA oxidation potential of the first recording (black). Subsequent recordings are colored to reflect the progression of time until concluding with red.

Activity on the Electrode Surface

As discussed previously, fouling of the electrode is a product of electroactive compounds becoming adsorbed to the surface resulting in decreased sensitivity. These compounds, including melatonin, persist on the surface for an extended period of time unless removed. As explored in Takmakov et al. (2010), CFmes can renew their surface given the right parameters. They found that application of a voltage greater than 1.0V will cause carbon on the surface of the electrode to degrade via oxidation of carbon into CO_2, slowly renewing the surface. It was also discussed that the application of a more traditional waveform (-0.4V-1.3V, 400V/s) will almost completely restore the sensitivity of an electrode in 15 minutes when cycled at 60Hz. By calculating the total time this waveform spends renewing its surface in 15 minutes, we are able to create a benchmark for how long the FSCAV and melatonin specific waveform should take to renew their electrode surface.

$$\frac{Total\ Voltage\ Above\ 1.0V}{Scan\ Rate} \times Scan\ Frequency \times 60\ Seconds\ \times 15\ Minutes$$

Based on the work done by (Takmakov et al., 2010) and the above equation, we believe that 81 seconds spent above 1.0V is the standard for which to compare to our waveforms tested. Using the same equation to assess the experimental waveforms finds that in the same 15-minute period the FSCAV waveform spends 45 seconds cleaning its surface and the melatonin specific waveform only spends 9 seconds. This means that the time it takes for the FSCAV and melatonin specific waveforms to sufficiently renew their surfaces would require 27 minutes and 135 minutes, respectively. Given that we

allocated 60 minutes for the washout period in the absence of melatonin this reasoning gives evidence that any changes, or lack thereof, in Dmax observed with the FSCAV waveform after 27 minutes is likely a function of biological action. However, the same cannot be said for the melatonin specific waveform.

Using these required times for surface renewal brings additional context for the background data displayed in **Figures 8 and 9**. As we have concluded, both the FSCAV and Melatonin specific waveforms experience a degree of fouling contributing to the decrease and positive shift in background signal after 1 hour of melatonin exposure (red line). The capability of the electrode to renew its surface can be observed by the restoration of the background signal back to baseline 1 hour after removal of melatonin from the aCSF buffer (blue line). The restoration rate which we calculated is consistent with what is seen for the melatonin specific waveform, with the background returning to approximately half of what it was before melatonin exposure. This persistent depreciated background current indicates that the final recordings of Dmax taken with the melatonin specific waveform are likely not entirely accurate due to some fouling still present on the CFme.

This is not the case for the FSCAV waveform, where the background current experiences a full recovery or, in many cases, exceeds the baseline. To reiterate, it was calculated that the surface would renew itself in less than a half hour. Given the hour washout period, it is not surprising that the background current is restored. The implications of this is that the final recordings taken with the FSCAV waveform should be a reasonably accurate representation of the biological change in DA release. As for

an explanation of the observed background exceeding baseline, it is likely a product of CFme etching also explored in depth by Takmakov et al. (2010). Background current is linearly proportional to scan rate and electrode surface area. As the CFme surface continues to renew itself, carbon is lost in the form of CO_2 and the morphology of the surface transitions from smooth to rough. Since roughening of the surface increases the surface area, the increased background current follows suit.

Outlier data

One data set which did not follow expected trends was the behavior of DA release observed during 10μM melatonin exposure when recording with the FSCAV waveform. Only one of our three slices tested experienced the expected pattern of decreased Dmax with minor restoration, while the other two actually experienced a moderate increase in Dmax upon melatonin exposure with little change into the washout period. Considering that this phenomenon occurred twice in the same test group, we believe there is more to the explanation besides possible error in procedure. Upon consultation of the literature, the contributor we believe to be at play is the diurnal expression of the MT1 receptor.

Much like the circadian role melatonin plays in the body, the MT1 receptor itself is under diurnal expression. Real-time PCR and western immunoblotting analysis have found low MT1 mRNA presence at night, but high MT1 receptor expression. Expression is inverse into daylight hours, with high MT1 mRNA and low MT1 receptor expression

(Uz et al., 2005). This information is important to discuss when retroactively considering the times of mouse sacrifice before experimentation.

As described in the methods, our mouse model was treated with a standard 12-hour day-night cycle of light exposure beginning at 7am. Due to extensive time frame of experiments we often began preparation as early as 8am. However, equipment troubleshooting in the early stages could delay an animal sacrifice up to 3 hours into the light cycle. Therefore, it is possible that the lack of consistent decrease in Dmax among experimental groups exposed to 10μM melatonin could be attributed to the varied expression of the MT1 receptor. Additionally, similarity between and consistency within the experimental groups of 50μM and 100μM melatonin exposure suggest that 10μM melatonin may not be adequate to sufficiently saturate available MT1 receptors. While there are likely more complicated cellular mechanisms at play, sufficient receptor saturation and the role which circadian control has on MT1 receptor expression cannot be overlooked as possible contributors.

Variability

Another occurrence with a dearth of explanation is the disparity between the washout periods of the FSCAV waveform and amperometry. There is great support in the literature that amperometry is not susceptible to fouling (Patel, 2008). Therefore, we believe that the change in Dmax observed by amperometry is likely the most accurate representation of the biological response to melatonin. However, what we have difficulty describing is why the endpoint mean Dmax for FSCAV at 50μM and

100μM remain ~20% compared to the persistence of ~75% which amperometry displays. Assuming our argument for surface renewal of the FSCAV electrode is correct, the last 30 minutes of FSCAV washout should also present data of the true biological response. While we should consider the variation of spatial CFme placement in relation to MT1 receptor localization, consistency among respective waveform sets in response to melatonin suggest that the most likely variable at play is the waveforms themselves. FSCAV and amperometry are functionally different in how they interact with DA at an electrochemical level. Considering the complex nature of surface interactions on the CFme, the possible explanation for this disparity could warrant an entire research project of its own. For this thesis we will conclude that, regardless of fouling, waveform selection could produce varied results if you are gathering longitudinal proportional data as performed in this project.

Implications of results

A limitation of this study is simply the interpretation of a single product from what is a multivariate system of interaction. When considering the washout period there are actually two factors which can contribute to an observed restoration in Dmax. One is the removal of melatonin which would reduce impedance if the electrode is susceptible to fouling. However, the other should be a restoration in VGCC function as the inhibition of which is generally reversed over several seconds in normal synaptic regulation (Ford, 2014). If the extent of downstream effects by MT1 receptor activation only encompassed VGCC, then we would expect the 1 hour duration given during the washout period should be sufficient for a full recovery of Dmax. Since the Dmax remains

persistently impaired, even for amperometry recordings, then it is reasonable to suggest that the downstream effects of MT1 are possibly extending beyond just VGCC function. Perhaps the 1 hour of melatonin exposure is a sufficient time frame for MT1 activation to inhibit AC and reduce cAMP enough to downregulate downstream mechanisms relating to DA release. This hypothesis is supported by similar voltammetry results produced by tasimelteon exposure (**Figure 12B**).

Summary

Our results found that despite variability between waveforms, all recording methods observed a decrease in Dmax in response to melatonin exposure. Analysis of all waveforms grouped together finds that time has a significant effect on change in Dmax upon melatonin exposure. Predicted linear modeling revealed significant change occurring as soon as 25 minutes into the exposure period. The melatonin washout period did not experience the same significant effect of time, supporting the hypothesis that fouling would not be a primary contributor to a change in Dmax.

Voltammetry data provided insight on our selected waveforms' resistance to melatonin fouling. While the melatonin specific waveform has shown to be more resistant to fouling than FSCAV, the slow rate of surface renewal reduced the viability of end-point data. FSCAV, with a much faster surface renewal rate, still presented inconsistencies with amperometry. Amperometry, intended as a baseline for comparison due to its proven resistance to melatonin fouling, performed as expected with linear modeling suggesting the absence of fouling. While our initial goal was to

observe the acute effects of melatonin exposure on DA release, our results suggest that 1 hour of MT1 receptor activation may be long enough to elicit significant downregulation of mechanisms involved with DA availability.

Future Direction

Due to the complicated nature of voltammetry, studies which seek to investigate CFme surface interactions with analytes are valuable to the field. Our results suggest that observing proportional changes in Dmax could produce different results dependent on what waveform is utilized. Further exploration of this phenomenon through extensive buffer work would likely produce valuable knowledge for the field of voltammetry. Additionally, given the potential power this technique has on assessing the temporal response of cellular metabolism from receptor signaling, this experiment could benefit from extended amperometric study. Varying degrees of exposure and washout periods could give important insight to the time frame that metabolic action follows receptor signaling.

Validity of the results produced by this experiment could be tested by further study of the role which the presynaptic MT1 receptor plays on DA regulation. Based on our conclusions, performing a similar experiment on *ex vivo* tissue slices of MT1 receptor knockout mice should not produce the same effects.

Appendix A

Statistical Tables

Waveform	Melatonin [C]	Mean+SD Dmax % t=60	Mean+SD Dmax % t=120
FSCAV	10μM	106.7±52.2	127.5±66.5
	50μM	24.4±25.5	14.8±15.1
	100μM	7.7±6.6	16.4±19.3
Melatonin-Specific	10μM	53.3±23.7	69.8±60.0
	50μM	12.9±5.2	34.1±12.8
	100μM	20.6±16.6	39.8±18.6
Amperometry	10μM	80.0±25.6	78.8±27.3
	50μM	53.6±30.4	68.4±28.3
	100μM	62.0±3.4	76.1±15.4

Table 1. Mean final Dmax for melatonin exposure and washout periods: summarized Mean and standard deviation for the final data collection of exposure (t=60) and washout (t=120) periods.

Analysis of GEE Parameter Estimates								
Empirical Standard Error Estimates								
Parameter			Estimate	Standard Error	95% Confidence Limits		Z	Pr > |Z|
Intercept			0.9884	0.1575	0.6797	1.2972	6.27	<.0001
WF	Amperometry		-0.2310	0.1586	-0.5418	0.0799	-1.46	0.1453
WF	FSCAV		-0.1193	0.1784	-0.4690	0.2303	-0.67	0.5035
WF	Melatonin		0.0000	0.0000	0.0000	0.0000	.	.
time			-0.0773	0.0099	-0.0967	-0.0579	-7.82	<.0001
Concentration	10		0.0736	0.1695	-0.2586	0.4058	0.43	0.6641
Concentration	50		-0.0621	0.1858	-0.4262	0.3020	-0.33	0.7381
Concentration	100		0.0000	0.0000	0.0000	0.0000	.	.
time*Concentration	10		0.0269	0.0102	0.0070	0.0469	2.65	0.0081
time*Concentration	50		-0.0052	0.0127	-0.0301	0.0198	-0.41	0.6835
time*Concentration	100		0.0000	0.0000	0.0000	0.0000	.	.
time*WF	Amperometry		0.0600	0.0105	0.0395	0.0805	5.74	<.0001
time*WF	FSCAV		-0.0027	0.0106	-0.0235	0.0181	-0.26	0.7981
time*WF	Melatonin		0.0000	0.0000	0.0000	0.0000	.	.
Concentration*WF	10	Amperometry	0.0735	0.1763	-0.2721	0.4191	0.42	0.6767
Concentration*WF	10	FSCAV	0.3059	0.2212	-0.1278	0.7395	1.38	0.1668
Concentration*WF	10	Melatonin	0.0000	0.0000	0.0000	0.0000	.	.
Concentration*WF	50	Amperometry	0.1032	0.2027	-0.2941	0.5006	0.51	0.6106
Concentration*WF	50	FSCAV	0.0952	0.2392	-0.3736	0.5640	0.40	0.6907
Concentration*WF	50	Melatonin	0.0000	0.0000	0.0000	0.0000	.	.
Concentration*WF	100	Amperometry	0.0000	0.0000	0.0000	0.0000	.	.
Concentration*WF	100	FSCAV	0.0000	0.0000	0.0000	0.0000	.	.
Concentration*WF	100	Melatonin	0.0000	0.0000	0.0000	0.0000	.	.
time*Concentration*WF	10	Amperometry	-0.0169	0.0124	-0.0412	0.0075	-1.36	0.1745
time*Concentration*WF	10	FSCAV	0.0427	0.0200	0.0034	0.0819	2.13	0.0333
time*Concentration*WF	10	Melatonin	0.0000	0.0000	0.0000	0.0000	.	.
time*Concentration*WF	50	Amperometry	-0.0071	0.0158	-0.0381	0.0240	-0.45	0.6555
time*Concentration*WF	50	FSCAV	0.0282	0.0180	-0.0070	0.0634	1.57	0.1161
time*Concentration*WF	50	Melatonin	0.0000	0.0000	0.0000	0.0000	.	.
time*Concentration*WF	100	Amperometry	0.0000	0.0000	0.0000	0.0000	.	.
time*Concentration*WF	100	FSCAV	0.0000	0.0000	0.0000	0.0000	.	.
time*Concentration*WF	100	Melatonin	0.0000	0.0000	0.0000	0.0000	.	.

Table 2. GEE parameter estimates for melatonin exposure period

Analysis of GEE Parameter Estimates								
Empirical Standard Error Estimates								
Parameter			Estimate	Standard Error	95% Confidence Limits		Z	Pr > |Z|
Intercept			0.1655	0.0713	0.0257	0.3052	2.32	0.0204
WF	Amperometry		0.6488	0.1019	0.4490	0.8485	6.37	<.0001
WF	FSCAV		-0.0571	0.0824	-0.2187	0.1044	-0.69	0.4883
WF	Melatonin		0.0000	0.0000	0.0000	0.0000	.	.
time			0.0217	0.0017	0.0183	0.0251	12.58	<.0001
Concentration	10		0.3886	0.1681	0.0591	0.7182	2.31	0.0208
Concentration	50		-0.0717	0.0747	-0.2181	0.0747	-0.96	0.3372
Concentration	100		0.0000	0.0000	0.0000	0.0000	.	.
time*Concentration	10		-0.0072	0.0116	-0.0299	0.0156	-0.62	0.5371
time*Concentration	50		0.0001	0.0040	-0.0078	0.0080	0.03	0.9765
time*Concentration	100		0.0000	0.0000	0.0000	0.0000	.	.
time*WF	Amperometry		-0.0235	0.0022	-0.0278	-0.0193	-10.75	<.0001
time*WF	FSCAV		-0.0160	0.0044	-0.0246	-0.0073	-3.61	0.0003
time*WF	Melatonin		0.0000	0.0000	0.0000	0.0000	.	.
Concentration*WF	10	Amperometry	-0.3844	0.2103	-0.7966	0.0279	-1.83	0.0676
Concentration*WF	10	FSCAV	0.5517	0.2815	0.0001	1.1034	1.96	0.0500
Concentration*WF	10	Melatonin	0.0000	0.0000	0.0000	0.0000	.	.
Concentration*WF	50	Amperometry	-0.0811	0.2244	-0.5208	0.3586	-0.36	0.7178
Concentration*WF	50	FSCAV	0.1539	0.1144	-0.0703	0.3781	1.35	0.1786
Concentration*WF	50	Melatonin	0.0000	0.0000	0.0000	0.0000	.	.
Concentration*WF	100	Amperometry	0.0000	0.0000	0.0000	0.0000	.	.
Concentration*WF	100	FSCAV	0.0000	0.0000	0.0000	0.0000	.	.
Concentration*WF	100	Melatonin	0.0000	0.0000	0.0000	0.0000	.	.
time*Concentration*WF	10	Amperometry	0.0076	0.0119	-0.0157	0.0310	0.64	0.5228
time*Concentration*WF	10	FSCAV	0.0276	0.0147	-0.0012	0.0564	1.88	0.0603
time*Concentration*WF	10	Melatonin	0.0000	0.0000	0.0000	0.0000	.	.
time*Concentration*WF	50	Amperometry	0.0036	0.0119	-0.0198	0.0270	0.30	0.7641
time*Concentration*WF	50	FSCAV	-0.0100	0.0108	-0.0312	0.0113	-0.92	0.3575
time*Concentration*WF	50	Melatonin	0.0000	0.0000	0.0000	0.0000	.	.
time*Concentration*WF	100	Amperometry	0.0000	0.0000	0.0000	0.0000	.	.
time*Concentration*WF	100	FSCAV	0.0000	0.0000	0.0000	0.0000	.	.
time*Concentration*WF	100	Melatonin	0.0000	0.0000	0.0000	0.0000	.	.

Table 3. GEE parameter estimates for melatonin washout period

Wald Statistics for Type 3 GEE Analysis			
Source	**DF**	**Chi-Square**	**Pr > ChiSq**
WF	2	10.69	0.0048
time	1	229.46	<.0001
Concentration	2	10.06	0.0065
time*Concentration	2	26.60	<.0001
time*WF	2	83.71	<.0001
Concentration*WF	4	2.97	0.5629
time*Concentration*WF	4	15.19	0.0043

Table 4. Output of GEE analysis of melatonin exposure period: Significance of DA release ratios as a function of waveform (WF), time, and concentration of melatonin

Wald Statistics for Type 3 GEE Analysis			
Source	**DF**	**Chi-Square**	**Pr > ChiSq**
WF	2	26.06	<.0001
time	1	16.07	<.0001
Concentration	2	20.40	<.0001
time*Concentration	2	1.07	0.5865
time*WF	2	12.64	0.0018
Concentration*WF	4	15.62	0.0036
time*Concentration*WF	4	7.11	0.1304

Table 5. Output of GEE analysis of melatonin washout period: Significance of DA release ratios as a function of waveform (WF), time, and concentration of melatonin.

Analysis Variable : DA Release										
Concentration	WF	N	Mean	Std Dev	Lower 95% CL for Mean	Upper 95% CL for Mean	Coeff of Variation	Minimum	Median	Maximum
10	Amperometry	36	0.86	0.17	0.80	0.91	19.31	0.57	0.84	1.08
	FSCAV	36	1.18	0.42	1.04	1.32	35.46	0.69	0.95	2.03
	Melatonin	36	0.73	0.25	0.65	0.82	33.49	0.27	0.73	1.54
50	Amperometry	36	0.61	0.25	0.52	0.69	40.97	0.20	0.71	1.01
	FSCAV	36	0.53	0.33	0.42	0.64	61.77	0.04	0.47	1.11
	Melatonin	36	0.39	0.36	0.27	0.51	92.14	0.06	0.25	1.45
100	Amperometry	36	0.64	0.15	0.59	0.70	23.73	0.44	0.63	1.28
	FSCAV	36	0.35	0.33	0.24	0.46	96.00	0.01	0.23	1.14
	Melatonin	36	0.49	0.35	0.37	0.61	72.70	0.10	0.40	1.48

Table 6. Descriptive statistics of DA release by concentration and waveform (WF) during melatonin exposure period: Each subgroup value is derived from an N=3. Each N was normalized by dividing the value by average of the pre-melatonin recordings for that experiment.

Analysis Variable : DA Release										
Concentration	WF	N	Mean	Std Dev	Lower 95% CL for Mean	Upper 95% CL for Mean	Coeff of Variation	Minimum	Median	Maximum
10	Amperometry	36	0.81	0.20	0.74	0.88	25.12	0.55	0.76	1.09
	FSCAV	36	1.22	0.49	1.05	1.38	39.93	0.63	1.12	2.17
	Melatonin	36	0.65	0.41	0.51	0.79	62.72	0.09	0.69	1.29
50	Amperometry	36	0.67	0.27	0.58	0.77	40.69	0.21	0.56	1.16
	FSCAV	36	0.16	0.11	0.13	0.20	69.32	0.02	0.17	0.38
	Melatonin	36	0.24	0.12	0.20	0.27	49.27	0.06	0.22	0.48
100	Amperometry	36	0.80	0.13	0.76	0.85	16.45	0.61	0.78	1.09
	FSCAV	36	0.15	0.13	0.10	0.19	86.45	0.01	0.09	0.39
	Melatonin	36	0.31	0.16	0.25	0.36	52.95	0.08	0.26	0.61

Table 7. Descriptive statistics of DA release by concentration and waveform (WF) during melatonin washout period: Each subgroup value is derived from an N=3. Each N was normalized by dividing the value by average of the pre-melatonin recordings for that experiment.

Time (min)	Waveform	Concentration	Conc*Waveform	Remark on interaction term
5	5.40, 2, 0.0673	1.19, 2, 0.5513	8.86, 4, 0.0646	Not Significant
10	8.01, 2, 0.0182	10.63, 2, 0.0049	2.20, 4, 0.6987	Not Significant
15	2.26, 2, 0.3229	17.02, 2, 0.0002	8.12, 4, 0.0872	Not Significant
20	1.09, 2, 0.5811	24.22, 2, <.0001	8.54, 4, 0.0737	Not Significant
25	4.23, 2, 0.1206	23.26, 2, <.0001	10.06, 4, 0.0395	Significant
30	8.94, 2, 0.0115	23.39, 2, <.0001	11.95, 4, 0.0177	Significant
35	18.25, 2, 0.0001	22.46, 2, <.0001	7.36, 4, 0.1182	Not Significant
40	24.72, 2, <.0001	21.17, 2, <.0001	12.08, 4, 0.0168	Significant
45	31.67, 2, <.0001	24.09, 2, <.0001	10.03, 4, 0.0399	Significant
50	25.03, 2, <.0001	32.14, 2, <.0001	9.70, 4, 0.0458	Significant
55	22.64, 2, <.0001	28.42, 2, <.0001	13.12, 4, 0.0107	Significant
60	21.87, 2, <.0001	23.68, 2, <.0001	11.27, 4, 0.0237	Significant

Table 8. Wald statistics for each time point during melatonin exposure period: Values given are in the order of Chi-square, degrees of freedom, and P-value.

	FSCAV 10	FSCAV 50	FSCAV 100	Mel 10	Mel 50	Mel 100	Amp 10	Amp 50	Amp 100
FSCAV 10		-1.0550	-1.0732	-0.5702	-0.9832	-0.9123	-0.4094	-0.5453	-0.4165
FSCAV 50	<.0001*		-0.0182	0.4848	0.0179	0.1428	0.6456	0.5098	0.6385
FSCAV 100	<.0001*	0.8339		0.5030	0.0900	0.1609	0.6638	0.5279	0.6567
Mel 10	0.0986	0.0364*	0.0324*		-0.4129	-0.3420	0.1608	0.0250	0.1537
Mel 50	0.0002*	0.3081	0.2677	0.0722		0.0709	0.5738	0.4379	0.5667
Mel 100	0.0009*	0.1419	0.1262	0.1528	0.4429		0.5028	0.3670	0.4957
Amp 10	0.1516	<.0001*	<.0001*	0.5241	<.0001*	0.0003*		-0.1359	-0.0071
Amp 50	0.0702	0.0013*	0.0013*	0.9263	0.0049*	0.0304*	0.4693		0.1287
Amp 100	0.1239	<.0001*	<.0001*	0.5143	<.0001*	<.0001*	0.9575	0.4337	

Table 9. Predicted mean and P-value for interaction of concentration and waveform over melatonin washout period. P-values which indicate significant difference between two data sets are denoted by (*).

References

Bassani, T. B., Gradowski, R. W., Zaminelli, T., Barbiero, J. K., Santiago, R. M., Boschen, S. L., … Vital, M. A. B. F. (2014). Neuroprotective and antidepressant-like effects of melatonin in a rotenone-induced Parkinson's disease model in rats. *Brain Research, 1593,* 95–105. https://doi.org/10.1016/j.brainres.2014.09.068

Benleulmi-Chaachoua, A., Chen, L., Sokolina, K., Wong, V., Jurisica, I., Emerit, M., … Zamponi, G. (2015). Protein interactome mining defines melatonin MT1 receptors as integral component of presynaptic protein complexes of neurons. *Journal of Pineal Research,* (60), 95–108. https://doi.org/10.1111/jpi.12294

Budygin, E. A., Oleson, E. B., Mathews, T. A., Läck, A. K., Diaz, M. R., McCool, B. A., & Jones, S. R. (2007). Effects of chronic alcohol exposure on DA uptake in rat nucleus accumbens and caudate putamen. *Psychopharmacology; Heidelberg*, *193*(4), 495–501. http://dx.doi.org.ezproxy.gvsu.edu/10.1007/s00213-007-0812-1

Canevelli, M., Valletta, M., Trebbastoni, A., Sarli, G., D'Antonio, F., Tariciotti, L., … Bruno, G. (2016). Sundowning in Dementia: Clinical Relevance, Pathophysiological Determinants, and Therapeutic Approaches. *Frontiers in Medicine*, *3*. https://doi.org/10.3389/fmed.2016.00073

Carriere, C. H., Kang, N. H., & Niles, L. P. (2016). Chronic low-dose melatonin treatment maintains nigrostriatal integrity in an intrastriatal rotenone model of Parkinson's disease. *Brain Research, 1633,* 115–125. https://doi.org/10.1016/j.brainres.2015.12.036

Cipriani, G., Lucetti, C., Carlesi, C., Danti, S., & Nuti, A. (2015). Sundown syndrome and dementia. *European Geriatric Medicine*, *6*(4), 375–380. https://doi.org/10.1016/j.eurger.2015.03.006

Dagher, A., & Robbins, T. W. (2009). Personality, Addiction, DA: Insights from Parkinson's Disease. *Neuron*, *61*(4), 502–510. https://doi.org/10.1016/j.neuron.2009.01.031

De Mei, C., Ramos, M., Iitaka, C., & Borrelli, E. (2009). Getting specialized: presynaptic and postsynaptic DA D2 receptors. *Current Opinion in Pharmacology*, *9*(1), 53–58. https://doi.org/10.1016/j.coph.2008.12.002

Dhillon, S., & Clarke, M. (2014). Tasimelteon: First Global Approval. *Drugs*, *74*(4), 505–511. https://doi.org/10.1007/s40265-014-0200-1

Doya, K. (2002). Metalearning and neuromodulation. *Neural Networks*, *15*(4), 495–506. https://doi.org/10.1016/S0893-6080(02)00044-8

Dubocovich, M. L., Delagrange, P., Krause, D. N., Sugden, D., Cardinali, D. P., & Olcese, J. (2010). International Union of Basic and Clinical Pharmacology. LXXV. Nomenclature, Classification, and Pharmacology of G Protein-Coupled Melatonin Receptors. *Pharmacological Reviews*, *62*(3), 343–380. https://doi.org/10.1124/pr.110.002832

Ferris, M. J., España, R. A., Locke, J. L., Konstantopoulos, J. K., Rose, J. H., Chen, R., & Jones, S. R. (2014). DA transporters govern diurnal variation in extracellular DA tone. *Proceedings of the National Academy of Sciences*, *111*(26), E2751–E2759. https://doi.org/10.1073/pnas.1407935111

Flagel, S. B., Clark, J. J., Robinson, T. E., Mayo, L., Czuj, A., Willuhn, I., … Akil, H. (2011). A selective role for DA in stimulus-reward learning. *Nature*, *469*(7328), 53–57. https://doi.org/10.1038/nature09588

Ford, C. P. (2014). The role of D2-autoreceptors in regulating DA neuron activity and transmission. *Neuroscience*, *282*, 13–22. https://doi.org/10.1016/j.neuroscience.2014.01.025

Franklin, K. B. J., & Paxinos, G. (2008). *The mouse brain in stereotaxic coordinates*. Academic Press.

Gratwicke, J., Jahanshahi, M., & Foltynie, T. (2015). Parkinson's disease dementia: a neural networks perspective. *Brain*, *138*(6), 1454–1476. https://doi.org/10.1093/brain/awv104

Hamdi, A. (1998). Melatonin administration increases the affinity of D2 DA receptors in the rat striatum. *Life Sciences*, *63*(23), 2115–2120. https://doi.org/10.1016/S0024-3205(99)80008-3

Hashemi, P., Dankoski, E. C., Lama, R., Wood, K. M., Takmakov, P., & Wightman, R. M. (2012). Brain DA and serotonin differ in regulation and its consequences. *Proceedings of the National Academy of Sciences of the United States of America*, *109*(29), 11510–11515. https://doi.org/10.1073/pnas.1201547109

Hazelton, L. (2006). Sundown Syndrome. In *The Encyclopedia of Aging* (4th ed.). Retrieved from https://search-credoreference-com.ezproxy.gvsu.edu/content/entry/spencage/sundown_syndrome/0

Heaulme, M., Leyris, R., Le Fur, G., & Soubrie, P. (1997). Involvement of potentially distinct neurotensin receptors in neurotensin-induced stimulation of striatal [3H]DA release evoked by KC1 versus electrical depolarization. *Neuropharmacology*, *36*(10), 1447–1454. https://doi.org/10.1016/S0028-3908(97)00131-7

Hensley, A. L., Colley, A. R., & Ross, A. E. (2018). Real-Time Detection of Melatonin Using Fast-Scan Cyclic Voltammetry. *Analytical Chemistry*, *90*(14), 8642–8650. https://doi.org/10.1021/acs.analchem.8b01976

Hermans, A., Keithley, R. B., Kita, J. M., Sombers, L. A., & Wightman, R. M. (2008). DA Detection with Fast-Scan Cyclic Voltammetry Used with Analog Background Subtraction. *Analytical Chemistry*, *80*(11), 4040–4048. https://doi.org/10.1021/ac800108j

Herr, N. R., Daniel, K. B., Belle, A. M., Carelli, R. M., & Wightman, R. M. (2010). Probing presynaptic regulation of extracellular DA with iontophoresis. *ACS Chemical Neuroscience*, *1*(9), 627–638. https://doi.org/10.1021/cn100056r

Howe, K., Clark, M. D., Torroja, C. F., Torrance, J., Berthelot, C., Muffato, M., … Whitehead, S. (2013). The zebrafish reference genome sequence and its relationship to the human genome. *Nature; London*, *496*(7446), 498–503.

Ilango, A., Shumake, J., Wetzel, W., Scheich, H., & Ohl, F. W. (2012). The Role of DA in the Context of Aversive Stimuli with Particular Reference to Acoustically Signaled Avoidance Learning. *Frontiers in Neuroscience*, *6*. https://doi.org/10.3389/fnins.2012.00132

Irwin, D. J., White, M. T., Toledo, J. B., Xie, S. X., Robinson, J. L., Deerlin, V. V., … Trojanowski, J. Q. (2012). Neuropathologic substrates of Parkinson disease dementia. *Annals of Neurology*, *72*(4), 587–598. https://doi.org/10.1002/ana.23659

Jones, L., McCutcheon, J., Young, A., & Norton, W. (2015). Neurochemical measurements in the zebrafish brain. *Frontiers in Behavioral Neuroscience*, 246. https://doi.org/10.3389/fnbeh.2015.00246

Kaslin, J., & Panula, P. (2001). Comparative anatomy of the histaminergic and other aminergic systems in zebrafish (Danio rerio). *Journal of Comparative Neurology*, *440*(4), 342–377. https://doi.org/10.1002/cne.1390

Kozaki, T., Kubokawa, A., Taketomi, R., & Hatae, K. (2015). Effects of day-time exposure to different light intensities on light-induced melatonin suppression at night. *Journal of Physiological Anthropology; Tokyo*, *34*. http://dx.doi.org.ezproxy.gvsu.edu/10.1186/s40101-015-0067-1

Mack, J. M., Schamne, M. G., Sampaio, T. B., Pértile, R. A. N., Fernandes, P. A. C. M., Markus, R. P., & Prediger, R. D. (2016). Melatoninergic System in Parkinson's Disease: From Neuroprotection to the Management of Motor and Nonmotor Symptoms. *Oxidative Medicine and Cellular Longevity; New York, 2016*. http://dx.doi.org.ezproxy.gvsu.edu/10.1155/2016/3472032

Marder, E., & Thirumalai, V. (2002). Cellular, synaptic and network effects of neuromodulation. *Neural Networks*, *15*(4), 479–493. https://doi.org/10.1016/S0893-6080(02)00043-6

Marsden, C. A. (2006). DA: the rewarding years. *British Journal of Pharmacology; London*, *147*(S1), S136-44. http://dx.doi.org.ezproxy.gvsu.edu/10.1038/sj.bjp.0706473

Meunier, C. J., Roberts, J. G., McCarty, G. S., & Sombers, L. A. (2017). Background Signal as an in Situ Predictor of DA Oxidation Potential: Improving Interpretation

of Fast-Scan Cyclic Voltammetry Data. *ACS Chemical Neuroscience*, *8*(2), 411–419. https://doi.org/10.1021/acschemneuro.6b00325

Moore, R. Y. (1995). Neural control of the pineal gland. *Behavioural Brain Research*, *73*(1–2), 125–130. https://doi.org/10.1016/0166-4328(96)00083-6

Naderi, M., Jamwal, A., Chivers, D. P., & Niyogi, S. (2016). Modulatory effects of DA receptors on associative learning performance in zebrafish (Danio rerio). *Behavioural Brain Research*, *303*, 109–119. https://doi.org/10.1016/j.bbr.2016.01.034

Naskar, A., Manivasagam, T., Chakraborty, J., Singh, R., Thomas, B., Dhanasekaran, M., & Mohanakumar, K. P. (2013). Melatonin synergizes with low doses of L-DOPA to improve dendritic spine density in the mouse striatum in experimental Parkinsonism. *Journal of Pineal Research*, *55*(3), 304–312. https://doi.org/10.1111/jpi.12076

Owen, G. R., & Brenner, E. A. (2012). Mapping Molecular Memory: Navigating the Cellular Pathways of Learning. *Cellular and Molecular Neurobiology*, *32*(6), 919–941. https://doi.org/10.1007/s10571-012-9836-0

Pandi-Perumal, S., BaHammam, A., Brown, G., Spence, D., Bharti, V., Kaur, C., … Cardinali, D. (2013). Melatonin Antioxidative Defense: Therapeutical Implications for Aging and Neurodegenerative Processes. *Neurotoxicity Research*, *23*(3), 267–300. https://doi.org/10.1007/s12640-012-9337-4

Paredes, D., Rada, P., Bonilla, E., Gonzalez, L. E., Parada, M., & Hernandez, L. (1999). Melatonin acts on the nucleus accumbens to increase acetylcholine release and

modify the motor activity pattern of rats. *Brain Research*, *850*(1), 14–20. https://doi.org/10.1016/S0006-8993(99)01992-7

Patel, B. A. (2008). Continuous amperometric detection of co-released serotonin and melatonin from the mucosa in the ileum. *The Analyst*, *133*(4), 516. https://doi.org/10.1039/b717034c

Patki, G., & Lau, Y.-S. (2011). Melatonin protects against neurobehavioral and mitochondrial deficits in a chronic mouse model of Parkinson's disease. *Pharmacology Biochemistry and Behavior*, *99*(4), 704–711. https://doi.org/10.1016/j.pbb.2011.06.026

Ramsson, E. S. (2016). A pipette-based calibration system for fast-scan cyclic voltammetry with fast response times. *BioTechniques*, *61*(5), 269.

Ramsson, E. S., Howard, C. D., Covey, D. P., & Garris, P. A. (2011). High doses of amphetamine augment, rather than disrupt, exocytotic DA release in the dorsal and ventral striatum of the anesthetized rat. *Journal of Neurochemistry*, *119*(6), 1162–1172. https://doi.org/10.1111/j.1471-4159.2011.07407.x

Randlett, O., Wee, C. L., Naumann, E. A., Nnaemeka, O., Schoppik, D., Fitzgerald, J. E., … Schier, A. F. (2015). Whole-brain activity mapping onto a zebrafish brain atlas. *Nature Methods*, *12*(11), 1039–1046. https://doi.org/10.1038/nmeth.3581

Shang, C., Li, X., Yin, C., Liu, B., Wang, Y., Zhou, Z., & Du, J. (2015). Amperometric Monitoring of Sensory-Evoked DA Release in Awake Larval Zebrafish. *Journal of Neuroscience*, *35*(46), 15291–15294. https://doi.org/10.1523/JNEUROSCI.3050-15.2015

Silva, M. W. B., Sousa-Muñoz, R. L., Frade, H. C., Fernandes, P. A., & Magalhães, A. de O. (2017). Sundown syndrome and symptoms of anxiety and depression in hospitalized elderly. *Dementia & Neuropsychologia*, *11*(2), 154–161. https://doi.org/10.1590/1980-57642016dn11-020008

Stone, K. L., & Tranah, G. J. (2017). Circadian Sleep-Wake Activity Patterns During Aging. In S. M. Jazwinski, V. P. Belancio, & S. M. Hill (Eds.), *Circadian Rhythms and Their Impact on Aging* (pp. 305–321). https://doi.org/10.1007/978-3-319-64543-8_13

Takmakov, P., Zachek, M. K., Keithley, R. B., Walsh, P. L., Donley, C., McCarty, G. S., & Wightman, R. M. (2010). Carbon Microelectrodes with a Renewable Surface. *Analytical Chemistry*, *82*(5), 2020–2028. https://doi.org/10.1021/ac902753x

Tay, T. L., Ronneberger, O., Ryu, S., Nitschke, R., & Driever, W. (2011). Comprehensive catecholaminergic projectome analysis reveals single-neuron integration of zebrafish ascending and descending Dopaminergic systems. *Nature Communications; London*, *2*, 171. http://dx.doi.org.ezproxy.gvsu.edu/10.1038/ncomms1171

Tellez, R., Gómez-Víquez, L., & Meneses, A. (2012). GABA, glutamate, DA and serotonin transporters expression on memory formation and amnesia. *Neurobiology of Learning and Memory*, *97*(2), 189–201. https://doi.org/10.1016/j.nlm.2011.12.002

Trotti, L. M., & Karroum, E. G. (2016). Melatonin for Sleep Disorders in Patients with Neurodegenerative Diseases. *Current Neurology and Neuroscience Reports*, *16*(7), 63. https://doi.org/10.1007/s11910-016-0664-3

Uz, T., Arslan, A. D., Kurtuncu, M., Imbesi, M., Akhisaroglu, M., Dwivedi, Y., … Manev, H. (2005). The regional and cellular expression profile of the melatonin receptor MT1 in the central Dopaminergic system. *Molecular Brain Research*, *136*(1), 45–53. https://doi.org/10.1016/j.molbrainres.2005.01.002

Valdés-Tovar, M., Estrada-Reyes, R., Solís-Chagoyán, H., Argueta, J., Dorantes-Barrón, A. M., Quero-Chávez, D., … Benítez-King, G. (2018). Circadian modulation of neuroplasticity by melatonin: a target in the treatment of depression. *British Journal of Pharmacology*, *175*(16), 3200–3208. https://doi.org/10.1111/bph.14197

Vallone, D., Picetti, R., & Borrelli, E. (2000). Structure and function of DA receptors. *Neuroscience & Biobehavioral Reviews*, *24*(1), 125–132. https://doi.org/10.1016/S0149-7634(99)00063-9

Wassum, K. M., & Phillips, P. E. M. (2015). Probing the Neurochemical Correlates of Motivation and Decision Making. *ACS Chemical Neuroscience*, *6*(1), 11–13. https://doi.org/10.1021/cn500322y

Willis, G. L., & Armstrong, S. M. (1999). A Therapeutic Role For Melatonin Antagonism in Experimental Models of Parkinson's Disease. *Physiology & Behavior*, *66*(5), 785–795. https://doi.org/10.1016/S0031-9384(99)00023-2

Xu, X., Weber, D., Carvan, M. J., Coppens, R., Lamb, C., Goetz, S., & Schaefer, L. A. (2012). Comparison of neurobehavioral effects of methylmercury exposure in older and younger adult zebrafish (Danio rerio). *NeuroToxicology*, *33*(5), 1212–1218. https://doi.org/10.1016/j.neuro.2012.06.011

Yapo, C., Nair, A. G., Clement, L., Castro, L. R., Hellgren Kotaleski, J., & Vincent, P. (2017). Detection of phasic DA by D1 and D2 striatal medium spiny neurons: Comparison of D1 and D2 responsiveness to transient DA. *The Journal of Physiology*, *595*(24), 7451–7475. https://doi.org/10.1113/JP274475

Yildirim, F. B., Ozsoy, O., Tanriover, G., Kaya, Y., Ogut, E., Gemici, B., … Aslan, M. (2014). Mechanism of the beneficial effect of melatonin in experimental Parkinson's disease. *Neurochemistry International*, *79*, 1–11. https://doi.org/10.1016/j.neuint.2014.09.005

Zachek, M. K., Hermans, A., Wightman, R. M., & McCarty, G. S. (2008). Electrochemical DA detection: Comparing gold and carbon fiber microelectrodes using background subtracted fast scan cyclic voltammetry. *Journal of Electroanalytical Chemistry*, *614*(1–2), 113–120. https://doi.org/10.1016/j.jelechem.2007.11.007

Zaitone, S. A., Hammad, L. N., & Farag, N. E. (2013). Antioxidant potential of melatonin enhances the response to L-dopa in 1-methyl 4-phenyl 1,2,3,6-tetrahydropyridine-parkinsonian mice. *Pharmacological Reports*, *65*(5), 1213–1226. https://doi.org/10.1016/S1734-1140(13)71479-8

Zisapel, N. (2001). Melatonin–DA Interactions: From Basic Neurochemistry to a Clinical Setting. *Cellular and Molecular Neurobiology*, *21*(6), 605–616. https://doi.org/10.1023/A:101518760